INVESTIGATE THE USAGE OF HEAT PIPE AS AIR CONDITIONING UNIT

LEE KAI FAN

UNIVERSITI TUNKU ABDUL RAHMAN

INVESTIGATE THE USAGE OF HEAT PIPE AS AIR CONDITIONING UNIT

LEE KAI FAN

A project report submitted in partial fulfilment of the requirements for the award of Bachelor of Engineering (Honours) Mechanical Engineering

Lee Kong Chian Faculty of Engineering and Science
Universiti Tunku Abdul Rahman

MAY 2022

DECLARATION

I hereby declare that this project report is based on my original work except for citations and quotations which have been duly acknowledged. I also declare that it has not been previously and concurrently submitted for any other degree or award at UTAR or other institutions.

Signature : 

Name : Lee Kai Fan

ID No. : 1702749

Date : 12/5/2022

APPROVAL FOR SUBMISSION

I certify that this project report entitled **"INVESTIGATE THE USAGE OF HEAT PIPE AS AIR CONDITIONING UNIT"** was prepared by **LEE KAI FAN** has met the required standard for submission in partial fulfilment of the requirements for the award of Bachelor of Engineering (Honours) Mechanical Engineering at Universiti Tunku Abdul Rahman.

Approved by,

Signature : 

Supervisor : Dr Wong Hong Mun

Date : 12/5/2022

ACKNOWLEDGEMENTS

I would like to thank everyone who had contributed to the successful completion of this project. I would like to express my gratitude to my research supervisor, Dr. Wong Hong Mun for his invaluable advice, guidance and his enormous patience throughout the development of the research.

In addition, I would also like to express my gratitude to my loving parents and friends who had helped and given me encouragement and emotional support throughout the project. I especially would like to express love towards my girlfriend, Ng Mei Yi, for her sacrifice in terms of time and contribution in terms of money.

Lastly, I would also like to thank Mr Ho, lab officer of Mechanical Workshop for assisting me in part of the construction of the prototype.

ABSTRACT

Solutions are provided by the heating, ventilating and air conditioning (HVAC) industry to improve the thermal comfort in the day to day lives of mankind. Conventional air conditioners and air cooler are commonly used to reduce the temperature of a space. In this final year project, the aim is to explore the concept of heat pipe air conditioner (HPAC). Heat pipes are passive heat transfer devices which relied on the phase change of its working fluid to remove heat, while air conditioners are devices which actively remove heat from a space via superheating its refrigerant. The hybridization of the two devices will allow a heat pipe to transfer heat actively. Once the concept of HPAC has been validated, this final year project will attract the interest of other researchers to further improve the current model. Optimistically, the HPAC can be introduced into the HVAC industry as a cheaper and more energy efficient alternative to air conditioner and air cooler. Two methods were formulated to validate the concept. One of the methods was to develop a mathematical model, which analysed the thermodynamic cycle of the HPAC. A prototype was also constructed to examine the cooling performance of the HPAC in actual conditions. In the mathematical model, it is shown that when the evaporator and condenser pressure were manipulated to the proper saturation pressure of the working fluid, heat transfer will occur. On the other hand, from the experiment, when isopropyl alcohol is used as working fluid, the evaporator experience significant increase in ΔT over time at low evaporator pressure (absolute pressure: 26 kPa to 60 kPa). The ΔT over time can be taken as an indicator of the cooling performance of the prototype. Hence, a significant increase in ΔT over time indicated that the prototype has performed cooling at low evaporator pressures. Lastly, the prototype performed the best at evaporator pressure of 26 kPa, when isopropyl alcohol, as the highest ΔT over time was recorded at 2.5 °C.

TABLE OF CONTENTS

LIST OF TABLES

LIST OF FIGURES

LIST OF SYMBOLS / ABBREVIATIONS

$\dot{Q}_H$	rate of heat exiting the condenser, kJ/s
$\dot{Q}_L$	rate of heat entering the evaporator, kJ/s
$\dot{m}$	mass flow rate of working fluid, kg/s
ΔP_c	*c*apillary pressure, Pa
ΔP_g	hydrostatic pressure drop
ΔP_{ll}	viscous pressure drop in the liquid line, Pa
ΔP_{vg}	vapor pressure drop in the grooves, Pa
ΔP_{vl}	viscous pressure drop in the vapor line, Pa
ΔP_w	liquid pressure drop in the wick, Pa
ΔT	difference between ambient and evaporator temperature, °C
h_f	enthalpy of fluid, kJ/(kg·K)
h_v	enthalpy of vapor, kJ/(kg·K)

AC	air conditioner
AHU	air handling unit
AHU	air handling unit
CC	compensation chamber
COP	coefficient of performance
CRAC	computer room air conditioning
CRAC	computer room air conditioning
CSPF	cooling seasonal performance factor
DOSM	Department of Standards Malaysia
EER	energy efficiency ratio
HPAC	heat pipe air conditioner
HPHE	heat pipe heat exchanger
HPSWH	heat pipes solar water heating systems
HVAC	heating, ventilating and air conditioning
IEQ	indoor environmental quality
LHP	loop heat pipe
LPG	liquified petroleum gas
VC	variable conductance

LIST OF APPENDICES

CHAPTER 1

INTRODUCTION

1.1 General Introduction

Air conditioner is a device used to maintain the temperature and humidity of an enclosed space (Legg, 2017). To maintain the setpoint conditions, air conditioner performed operations such as heating, cooling, humidifying, and dehumidifying. In some application, operations maybe combined to achieve the intended purpose such as cooling with dehumidification or heating with humidification (Cengel and Bole, 2015).

Regardless of the type of air conditioner, most of the air conditioners operate on vapor compression cycle (Chua et al., 2021). Vapor compression cycle relied on the phase change of its refrigerant to operate. In order to attain the heat transfer, the temperature and pressure of refrigerant is increased by a compressor, until the refrigerant is at superheated steam phase in the entrance of the condenser. Heat is released in the condenser. Subsequently, the temperature and pressure of refrigerant is reduced by passing through an expansion valve. The refrigerant entered the evaporator at a lower temperature than surrounding, hence ambient heat entered the evaporator thus providing cooling to the surrounding (Borgnakke and Sonntag, 2019). Figure 1.1 shows the schematic diagram and the thermodynamic cycle of a vapor compression cycle.

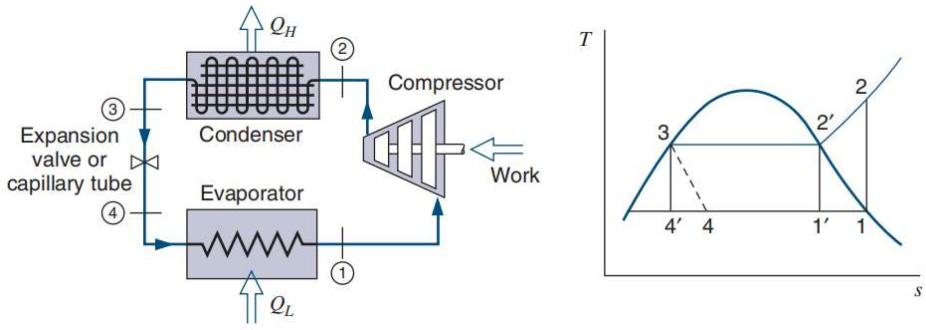

Figure 1.1: Schematic diagram and Temperature-Entropy diagram of vapor compression cycle (Borgnakke and Sonntag, 2019).

Air conditioners have a wide range of applications which can be commonly found in residential houses as single split and multi-split air conditioner, in commercial buildings as air handling unit and Variable Refrigerant Volume system, and in data centres as CRAC units (Capozzoli and Primiceri, 2015; Shahsavar Goldanlou, Kalbasi and Afrand, 2020; Wan et al., 2020).

This final year project report focused on alternative device to cool down a space. One of the devices in interest is the heat pipe. Heat pipe is a device which relied on the properties of fluid phase change to transport heat from the hot medium to a colder medium passively (Zohuri, 2016). A basic heat pipe consisted of a sealed and vacuumed envelope with a wick structure lined around the inner walls of the envelope and working fluid. The working principle of heat pipe will be reviewed in Chapter 2. However, based on Figure 1.2, a brief explanation of the working principle can be explained as such:

1. Heat entered the evaporator and vaporised the liquid phase working fluid.
2. Vapor working fluid escaped from wick and travelled to the condenser section via an adiabatic section.
3. Heat is released by the vapor working fluid at the condenser section and condensed back to liquid phase and transported via wick structure using capillary action to evaporator.

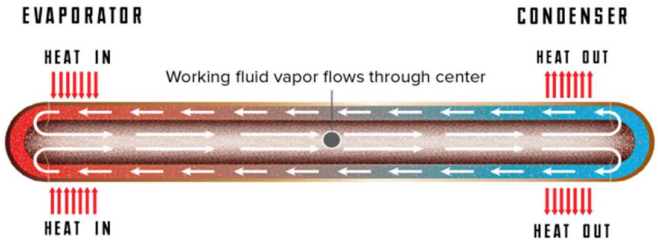

Figure 1.2: Schematic diagram of heat pipe (NCT, 2021).

Heat pipes are capable of transferring heat over a distance almost instantaneously, with minimal heat loss (Barrak, 2021). Hence, heat pipes are found in many applications such as electronics cooling, solar thermal water heating, energy recovery systems and heat pipe driven heat exchanger (Zohuri, 2020). There are various sorts of heat pipe catered for different purposes such as pulsating heat pipes, rotating, revolving heat pipes, capillary pumped loop

and loop heat pipe (Zohuri, 2016). In this final year project, feasibility of loop heat pipe (LHP) as air conditioning will be studied.

1.2 Importance of the Study

This final year project studied the feasibility of heat pipe air conditioner (HPAC) as a replacement to conventional air conditioner in low heat removal applications.

The two options for cooling a space, are conventional air conditioners and air coolers. Conventional air conditioners while effective in removing large amount of heat, can be costly to operate. This is because air conditioners used compressor to superheat the refrigerant in order to transfer heat, which consumed large amount of energy. On the other hand, air cooler provides sufficient heat removal at low operating cost. However, air coolers are less effective in humid environments as it operates on evaporative cooling. Water tanks inside the air cooler also presents as potential breeding ground for mosquitoes.

A HPAC may potentially provide a middle ground between conventional air conditioners and air cooler. If this study successfully proved the concept of HPAC, it may grasp interest from more researchers, and develop further on HPAC topic. Hopefully introducing HPAC into the HVAC market as an alternative to air conditioners and air cooler for consumers to improve their quality of living.

1.3 Problem Statement

Indoor environmental quality (IEQ) of an enclosed space is important for the health and comfort of the occupants. One of the aspects of IEQ is the thermal quality and it is heavily influenced by the outdoor environmental conditions. Malaysian experienced hot and humid weather all year round. While air conditioners can be used to cool a space down, it is often used to maintain a large temperature difference between indoor and outdoor. A simple yet low power consumption device may potentially replace the role of air conditioners to remove heat from an indoor environment. Heat pipes are passive heat transfer device, which does not require external power input to transfer heat making it ideal for home and office heat removal applications. However, heat pipe can

only transfer heat from hot medium to cold medium. HPAC should operate similar to air conditioners, which requires the HPAC to transfer heat from lower indoor temperature to higher outdoor temperature through modifications and hybridization.

1.4 Aim and Objectives

The aim of the study is to explore the concept of heat pipe air conditioner. Hence, to accomplish the aim of this study two objectives were developed as follow.

1. To model the use of heat pipe for air conditioning application.
2. To design and develop a proof of concept model of the heat pipe air conditioning system.

1.5 Scope and Limitation of the Study

This paper investigated the concept of HPAC. To validate the concept, mathematical modelling and prototyping will be carried out. Mathematical modelling was performed to determine the suitable working pressure and obtain the corresponding enthalpy of the working fluid from the property table to calculate the theoretical rate of heat transfer. The prototype was constructed to analyse the heat transfer rate of the HPAC model in real-life conditions. The performance of HPAC will also be evaluated in terms of its cooling performance. The increment of $\Delta T = T_{amb} - T_{evap}$ over time will be considered as the cooling performance of the prototype.

Various factors will influence the heat transfer capabilities of heat pipe such as the envelope material, diameter and orientation of the heat pipe, working fluid and structure of the condenser and evaporator. However, only the effect of different working fluid and evaporator pressure on the heat transfer performance was studied. Lastly, the experiment was carried out in an environment which was not controlled; hence, external factors may affect the data collected.

1.6 Contribution of the Study

Upon completion of this study, the concept of heat pipe air conditioner may be proven. Hence, this study will contribute to the world of researchers, providing a new and interesting topic to further explore in. Furthermore, if other researchers can increase the cooling capacity and efficiency of the heat pipe air

conditioner, then the concept of heat pipe air conditioner can be developed into an actual product which can be introduced to the consumer market. Hence, improving the quality of living in Malaysia.

1.7 Outline of the Report

Encompassed in this report are five chapters, starting from introduction, where a brief introduction was provided on air conditioning and heat pipes, problem statement, importance of study, aims and objectives, scope, limitation and contribution of the study. Following Chapter 1 is the literature review, where Chapter 2 begins with the review of literatures on the topic of LHP. Subsequently, the indoor environmental quality and thermal quality of an enclosed space is reviewed. Next, the fundamentals of LHP were explored. Lastly, in Chapter 2, the air conditioning process and thermodynamics of water were studied. In Chapter 3, a detailed methodology was displayed. It included the mathematical modelling and prototype construction process and experimental procedure. Subsequent, in Chapter 4, the results obtained from the experiment were tabulated. A detailed discussion was also included in Chapter 4 which analysed the data obtained from the experiment. The working principle of the heat pipe air conditioner and factors affecting the heat transfer rate were also discussed. There were also additional discussions attached to the appendix, which explains the necessity to replace the helical coil copper pipe on the evaporator side to a galvanised iron pipe. Lastly, Chapter 5 concluded and summarised the report.

CHAPTER 2

LITERATURE REVIEW

2.1 Introduction

This chapter will be separated into 4 subchapters. The first subchapter reviewed the indoor environmental quality (IEQ), thermal quality of an indoor environment. The second part of the literature review covered the fundamentals of LHP, which included the structure of LHP, working principles, operating limits, effect of fill ratio on the heat transfer capabilities of heat pipe, mathematical modelling of LHP and efforts of past researchers in integrating heat pipe in HVAC industry. The last two subchapters will cover psychometric chart, air conditioning process and thermodynamics of water.

Aono et al. (2021) investigated the application of LHP which has kilowatts heat transfer capabilities. The LHP was constructed using stainless steel and water is used as working fluid. In the experiment, the condenser tube diameter was varied between 1/2-inch and 3/4-inch. The results showed that the LHP with 1/2-inch condenser tube has the highest heat transport capability of 6200 W under natural water convection. Figure 2.1 shows the experimental setup of kW-class LHP constructed by them.

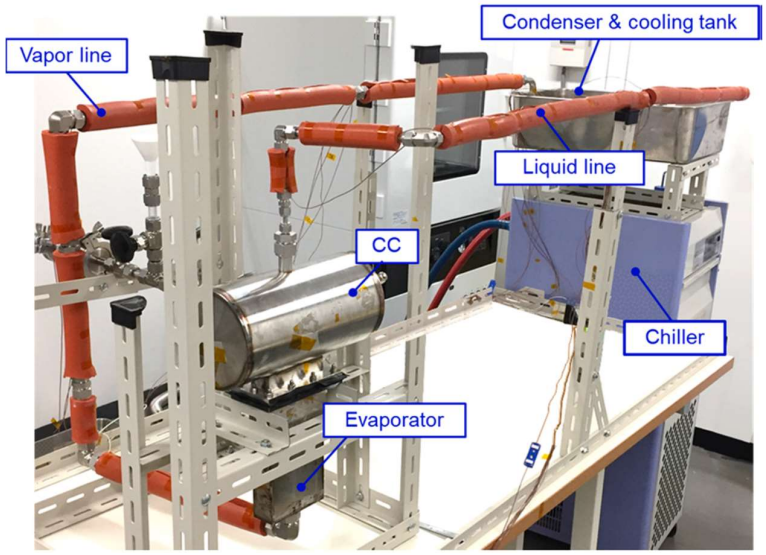

Figure 2.1: Experimental setup of kW-class LHP (Aono et al., 2021).

A pump driven LHP was developed by Zhang et al. (2020a); Zhou, Wei and Ma (2017); Setyawan et al. (2019), in attempts to overcome the heat transfer barriers of traditional LHP such as fluctuation in operating temperature and the restricted heat transfer distance. In the three research, the pump was integrated in between the evaporator and compensation chamber. The pump was used to assist the flow of working fluid, increase heat transfer capacity and stabilize the operating temperature. Zhang et al. (2020a) selected a centrifugal pump, which is capable of flow rate up to 2 L/min and producing 90 kPa of pressure (water). Figure 2.2 shows the schematic diagram of the LHP with integrated pump. Ammonia was selected as the working fluid as it prevents cavitation which may potentially damage the pump and is suitable for the researcher's application (Operating temperature:$-60\ °C\ to + 60\ °C$). Setyawan et al. (2019) opted for a diaphragm pump which has a flow rate varying between 40 ml/min to 100 ml/min. Setyawan et al. (2019) explained that the diaphragm pump was used to avoid dry-out conditions in the evaporator section of the LHP.

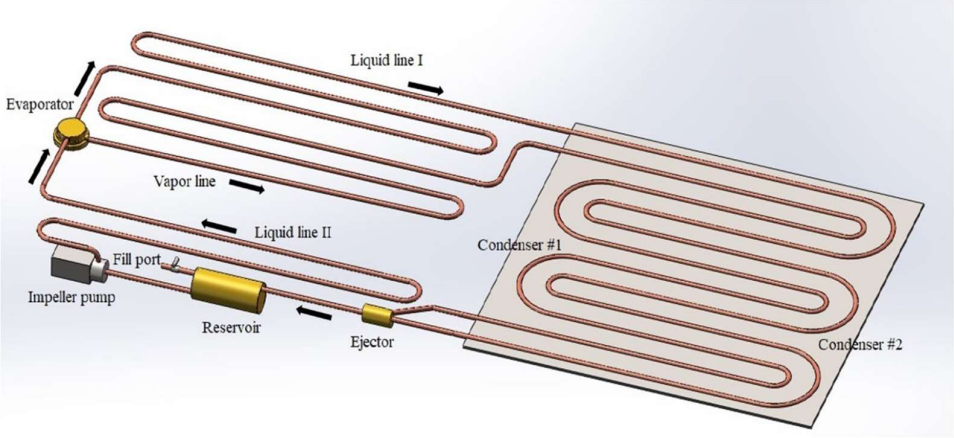

Figure 2.2: Diagram of the pump assisted LHP (Zhang et al., 2020a).

Zhang et al. (2020) and Setyawan et al. (2019) concluded that integrating a pump into the LHP shows an increase in the heat transfer performance and lowers the operating temperature. Zhang et al. (2020) also stated that installing a pump in LHP will assist in start-up operation of LHP at low heat load. Setyawan et al. (2019), however, concluded that integrated pump does not provide significant benefits at low heat loads. Zhou, Wei and Ma (2017) developed a pump-driven LHP to be implemented in as energy recovery

ventilators in buildings. The pump selected has a rating of 1.0 kW in power, maximum head of 57 m (water) and volumetric flow rate of 3 m^3/hr; R32 was used as working fluid. Zhou, Wei and Ma (2017) summarised the benefits of implementing pump-assisted loop heat in data centres which include energy savings compared to air conditioner.

Su et al. (2019) performed an experimental analysis on the feasibility of LHP to function as hydraulic cooling system and anti-icing device in aircrafts. To prevent the working fluid from freezing at sub-zero temperatures and to pertain high heat transfer capabilities of water, the working fluid used is a blend of 60% ethanol and 40 % water. From the experimental results, the authors concluded that LHP has high practicality in aircraft as an anti-icing device.

Wang et al. (2019) studied the effect of non-condensable gas and evaporator tilt on the performance of LHP. Figure 2.3 shows the cross sectional view of the evaporator and compensation chamber (CC) of the LHP. Figure 2.3 also shows the tilt angle of the LHP in relation to direction of gravity. The authors concluded that LHP has the worst performance when placed in -15° tilt and performed best when tilt is at $+15°$ regardless of the presence or absence of non-condensable gas. Non-condensable gas generally decreased the heat transfer performance of LHP as it tends to increase the operating temperature, nevertheless, adverse evaporator tilt conditions may impair the heat transfer capability more when compared to the effect of non-condensable gas.

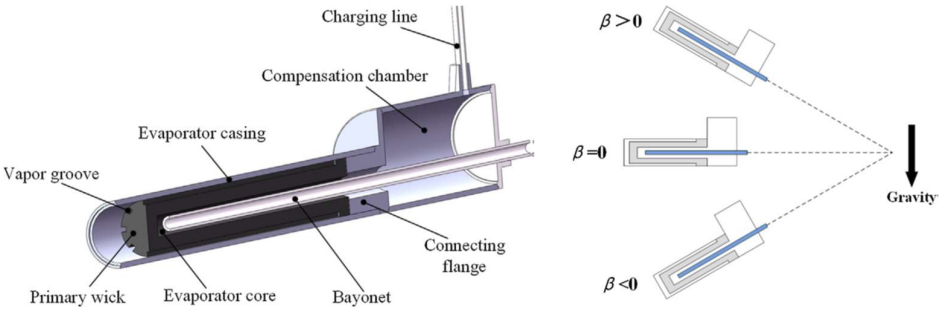

Figure 2.3: Cross sectional view of the CC and evaporator of LHP and the tilt angle of the LHP (Wang et al., 2019).

Bernagozzi et al. (2021) developed a cooling system for electrical vehicles using LHP. The evaporator of the LHP is placed under the battery cells while the condenser is thermally coupled to the existing cooling circuit of

HVAC. The goal of the novel cooling system is to reduce the complexity of cooling system and the reliance on active cooling system.

Shafieian and Khiadani (2020) investigated the benefits of heat pipes solar water heating systems (HPSWH). The results from the paper showed that HPSWH system was able to achieve average solar fraction of 0.983 in the summer and 0.427 in the winter. They also highlighted on the potential savings of LPG when implementing HPSWH system.

He et al. (2017); Enke, Bertoldo Júnior and Vlassov (2021) investigated the influence of non-condensable gas on the performance of heat pipe. He et al. (2017) investigated start-up performance of LHP based on four different start-up conditions were summarised in Table 2.1.

Table 2.1: Start-up conditions for LHP.

Condition	Phase of working fluid	
	Vapor Groove	Evaporator Core
1	Liquid	Liquid
2	Vapor	Liquid
3	Liquid	Vapor
4	Vapor	Vapor

He et al. (2017) performed the two sets of experiments with the four conditions one set is subjected to preconditioning while the other set is not subjected to preconditioning. The results showed that condition 2 failed to start-up, while non-condensable gas have negative effect on the start-up of condition 1 and 3. Lastly, non-condensable gas facilitated the start-up procedure of LHP in condition 4. He et al. (2017) also noted that only condition 1 was able to successfully start-up when LHP is subjected to precondition. Enke, Bertoldo Júnior and Vlassov (2021) also studied the transient response of heat pipe and confirmed the finding of He et al. (2017).

2.2 Indoor Environmental Quality

In the modern era, humans spend on average up to 90% of their time indoors (Kishi and Araki, 2020). Numerous studies have concluded that poor indoor environmental quality (IEQ) will lead to adverse health effects, which includes

sickness building syndrome, respiratory-related infections and allergies, and psychological effects such as fatigue, decrease productivity and low satisfaction (Mendes and Teixeira, 2014; Yang and Mak, 2020; Esfandiari et al., 2021). Hence, occupants should monitor their IEQ, as buildings with proper IEQ will enhance the quality of living, safeguard the health of the occupants and increase productivity of the occupants (Abdul Mujeebu, 2019). IEQ is a matrix used to evaluate the quality of an indoor environment with regards to the comfort and health of the occupants (Esfandiari et al., 2021). IEQ is strongly influenced by the interactions between biological factors such as fungi and bacteria, physical factors such as lighting, humidity, air circulation and temperature, and chemical factors such as harmful emission and pollutants present in the indoor environment (Ganesh et al., 2021). The four main physical factors to consider when improving IEQ are lighting quality, acoustics quality, indoor air quality and thermal quality (Wang et al., 2021). Besides that, IEQ may also be affected by the outdoor conditions, such as weather and direct ventilation, which may indirectly affect the indoor temperature and introduce pollutants from the outside environment to indoor (Toyinbo, 2019).

Due to the geographical location of Malaysia, the weather is hot and humid throughout the whole year; the daily mean temperature of Malaysia ranges from $21\ °C\ to\ 32\ °C$ (MyGovernment, 2016). Indoor temperature of a building is strongly correlated to its outdoor temperature; hence, thermal quality of a building would also be affected by the weather (Nguyen, Schwartz and Dockery, 2014; Asumadu-Sakyi et al., 2021). Several studies have been conducted to collect data on indoor temperatures of various types of buildings in Malaysia, which can be summarised in Table 2.2.

The perceived thermal quality differs among individuals. This is because thermal quality is governed by psychological and physiological factors (Abdul Mujeebu, 2019). Psychological factors depends on the individual's thermo-specific self-efficacy, emotional state and personality (Schweiker et al., 2018). Physiological factors can be classified into environmental and individual factors. Environmental factor is dependent on four criteria which are air temperature, air humidity, radiant temperature and air velocity; individual factors include clothing insulation and metabolic rates (ASHRAE, 2010; Akanmu, Nunayon and Eboson, 2021). Department of Standards Malaysia (DOSM) recommends

certain criteria for indoor environment to achieve thermal comfort, which is summarised in Table 2.3.

Table 2.2: Range of indoor temperature for various buildings.

Building Type	Location	Temperature Range	Researcher
Educational institution	Perak	$27.5\,°C - 32\,°C$	(Koh, Al-Kayiem and Kurnia, 2018)
Office Building	Kuala Lumpur	$29.5\,°C - 34\,°C$	(Arifin and Denan, 2015)
Mosque	Melaka	$29.5\,°C - 32.2\,°C$	(Yusoff and Ja'afar, 2019)
Residential	Kuala Lumpur	$27\,°C - 33\,°C$	(Wai Tuck et al., 2019)
	Negeri Sembilan	$29.2\,°C - 33\,°C$	(Amir et al., 2019)
	Kuala Lumpur	$27\,°C - 31\,°C$	(Zaki et al., 2018)
	Kuala Lumpur	$24\,°C - 32\,°C$	(Baharum et al., 2014)
	Kuala Lumpur	$29.5\,°C - 32.6\,°C$	(Jamaludin et al., 2015)
	Kuching	$28\,°C - 31.1\,°C$	
	Penang	$29.5\,°C - 31.6\,°C$	

Table 2.3: Conditions for indoor environment (Department of Standards Malaysia, 2014).

Component	Criteria
Air Temperature	$24\,°C - 26\,°C$
Relative Humidity	$50\% - 70\%$
Air Velocity	$0.15\,m/s - 0.5\,m/s$

As discussed earlier, when IEQ is neglected, undesirable health and psychological effects will occur; similarly, when thermal quality is overlooked, health risks such as heat stroke, cardiovascular and respiratory related

hospitalization and deaths may arise (Ormandy and Ezratty, 2016). Studies also showed deteriorated productivity, cognitive functions and sleep quality with the increased in temperatures (Geng et al., 2017; Cedeño Laurent et al., 2018). Therefore, in order to maintain indoor thermal quality at comfortable levels, occupants may opt for air conditioners. However, air conditioners are often used to create large temperature differential. According to the standards published by DOSM (2014), in some instances, when indoor temperature is decreased by 1 °C to 2 °C is sufficient to provide thermal comfort for the occupants. Hence, a modified LHP might be more suitable for removing heat to maintain temperature at optimum thermal quality level.

2.3 Fundamentals of Heat Pipe

There are many variations of heat pipe which are designed to overcome various limitation of the traditional heat pipe. The commonly found variations are variable conductance (VC) heat pipe, rotating heat pipe, pulsating heat pipe, thermosyphons, micro heat pipe and LHP (Zohuri, 2016; Sharma and Sharma, 2019).

The conventional heat pipe will self-adjust its operating temperature depending on the heat load. To ensure the evaporator side of a heat pipe is constant at a certain temperature, despite the fluctuating heat load, a VC heat pipe can be used (Zohuri, 2016; Jouhara, 2018). The thermal conductance of a VC heat pipe is controlled through either one of the four methods which are, excess liquid heat pipe, vapor or liquid flow modulated heat pipe and gas loaded heat pipe (Zohuri, 2016; Jouhara, 2018).

Micro LHP, thermosyphons, pulsating heat pipe and rotating heat pipe do not require the wick structure to operate. In order for the return of liquid working fluid from condenser section to evaporator section, thermosyphons rely on the effect of gravity while micro heat pipe and pulsating heat pipe rely on the structure of the pipe (Sharma and Sharma, 2019). The condenser of a thermosyphon is located above its evaporator, hence as the vapor working fluid condensed back to liquid phase, gravity will act on the liquid working fluid, which allowed the condensate to return to the evaporator (Abdullahi, Al-dadah and Mahmoud, 2019). Noncircular channel in the micro heat pipes is used for transportation of its working fluid (Qu et al., 2017; Jouhara, 2018). The channel

of a micro heat pipe consisted of sharp angle edges which provides the driving force in the form of capillary pressure (Jouhara, 2018). Figure 2.4 shows the various cross section shapes of the channel commonly found in micro heat pipe. The pulsating heat pipe takes the form of a closed loop. In pulsating heat pipe, liquid and vapor phase working fluid will travel in the same direction (Jouhara, 2018). When pulsating heat pipe received heat at the evaporator section, the liquid working fluid vaporised, which leads to the formation of vapor bubbles. As the vapor bubbles grow in size, the vapor pressure increased, which caused the working fluid to travel towards condenser section. At the condenser, as the heat in the working fluid is dissipated, the working fluid condensed causing the vapor bubble to collapse. This combination of action of formation and collapse of vapor bubble leads to the pulsating motion of working fluid (Alhuyi Nazari et al., 2018).

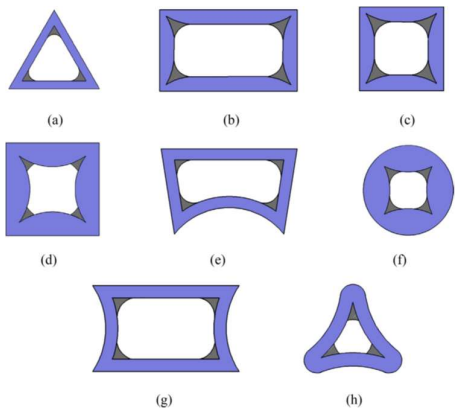

Figure 2.4: Cross section of micro heat pipe (Qu et al., 2017).

As of the current discussion, all of the heat pipes are static during operation. In other words, the heat pipe does not rely on motion of its structure to operate. As the name implies, the rotating heat pipe requires the heat pipe to be rotated around the axial or radial axis (Xie et al., 2015). Liquid phase working fluid is transported from the condenser to evaporator by the centrifugal forces created by the rotation of the heat pipe (Xie et al., 2015; Jouhara, 2018).

Regardless of the type of heat pipe, the operating principle is similar. Heat pipe are heat transfer device which operates on the phase change of its working fluid (Zohuri, 2016). When sufficient heat entered the evaporator, liquid working fluid then vaporised, absorbing the heat as latent heat of

vaporization. Therefore, removed heat around the vicinity of the evaporator. The vapor then moved to the condenser section where it condensed, releasing the latent heat of vaporization (Zohuri, 2016). The working fluid then travelled back to the evaporator via one of the mechanisms explained above.

2.3.1 Structure of Loop Heat Pipe

LHP has 5 fundamental components which are the evaporator, wick, condenser, transport line and compensation chamber (Zohuri, 2016; Guo, 2019). The wick is lined along the inner walls of the evaporator. The wick is a porous structure and contains working fluid in liquid phase (Zohuri, 2016). Heat entered the LHP through the evaporator envelope and conducted to the wick. Compensation chamber is hydrodynamically and thermally coupled to the core of evaporator, hence can be consider as an extension of core of the evaporator (Ambirajan et al., 2012). A compensation chamber is a reservoir, which accommodates the fluid volume for two purposes. When temperature of working fluid fluctuates, compensation chamber accommodates the change in density (Ambirajan et al., 2012). Depending on the heat load, compensation chamber will either replenished or received working fluid with the condenser, in turn facilitates the varying of conductor conductance (Ambirajan et al., 2012; Zohuri, 2016). In a LHP, a condenser can be a conventional heat exchanger such as air-cooled, pipe in pipe, plate heat exchanger depending on the application (Edreis and Petrov, 2020). Vapor phase working fluid released heat to a heat sink via the heat exchanger. Transport line consisted of the vapor and liquid line. Transport lines are smoothed wall pipe, which coupled the evaporator and condenser. Liquid phase working fluid is transported from the condenser to the compensation chamber via liquid line, while vapor phase working fluid is transported from evaporator to the condenser via vapor line (Ambirajan et al., 2012). Figure 2.5 shows the components of a miniature LHP, while Figure 2.6 shows the cross sectional view of a flat shaped evaporator of a LHP.

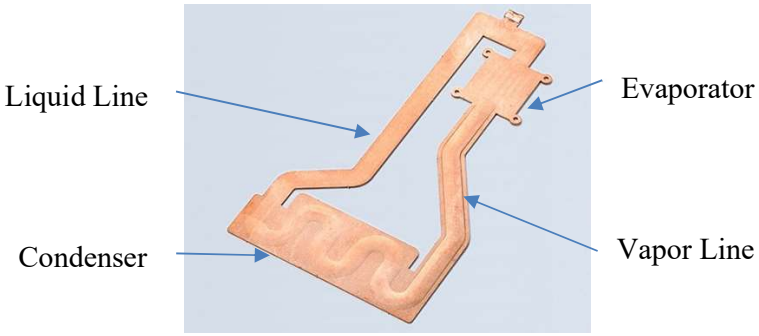

Figure 2.5: Miniature LHP (Shinko Electric Industries, 2021).

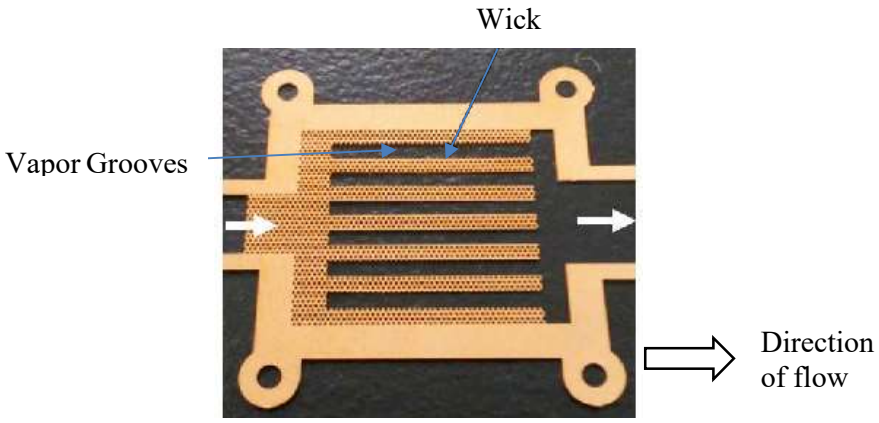

Figure 2.6: Cross section of flat shaped evaporator of LHP (Shioga and Mizuno, 2015).

2.3.2 Working Principle of Loop Heat Pipe

In this section, the steady state operation of LHP is studied. The LHP is assumed to have an ideal start-up. As mentioned earlier, LHP operates based on multi-phased fluid flow cycle. LHP transports heat in the form of latent heat of vaporization, which required the phase change of the working fluid. Because of the operating principle of LHP, the temperature difference in the loop is small (2 °C - 5 °C).

The assumptions for ideal start-up are the vapor groove is filled up with vapor and evaporator core is filled up with liquid (Jose and Baby, 2018; Barbosa and Mantelli, 2021). During start-up transient, heat outflow to the compensation chamber from the evaporator is assumed to be small because wick would have a high thermal resistance which prevent large temperature overshoot (Reay, Kew and McGlen, 2014b; Ku, 2016). After, the cooled liquid from the condenser reached the compensation chamber, temperature in the compensation chamber decreased and the loop will reach its steady state (Ku, 2016). The two

characteristic which determine the quality of start-up are the temperature overshoot and the start-up time. Temperature overshoot described difference in temperature between the maximum temperature the evaporator obtained during start-up (prior to the flow of working fluid in the loop) and the steady state operating temperature of the evaporator. Start-up time is defined as the time required for the initiation of circulation of working fluid in the LHP when heat is initially applied (Ku, 2016). The standard for a good start-up would be having a start-up time of less than 3 minutes and a temperature overshoot of less than 5 $°C$ (Ambirajan et al., 2012). Figure 2.7 shows the schematic diagram of a LHP, direction of heat travel, and the direct of travel of working fluid.

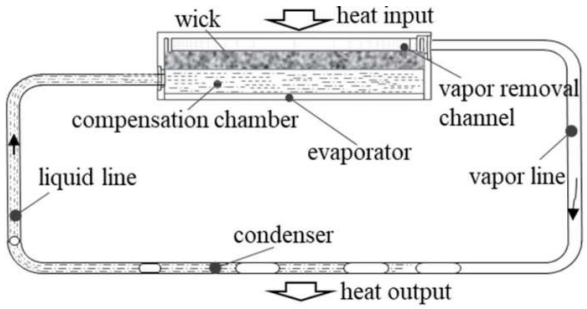

Figure 2.7: Schematic Diagram of LHP (Cai et al., 2021).

During steady-state operation, the heat applied to evaporator envelope, is absorbed by the liquid working fluid at the wick surface. The working fluid evaporated, absorbing the heat as latent heat of vaporization (Zohuri, 2016). The backflow of vapor from evaporator to the compensation chamber is inhibited by the capillary forces in the wick (Ambirajan et al., 2012). Hence, the vapor generated will travelled outwards from the wick to the vapor grooves, which are located at the inner evaporator walls. Vapor grooves are small channels which removed the vapor generated in the wick and transport the vapor to the vapor lines or in some application the vapor removal channel (Reay, Kew and McGlen, 2014b). Vapor grooves ensure the pressure drop caused by flow of vapor from wick to the vapor line is within an acceptable range. As vapor is removed from the wick, the surface tension of fluid in the meniscus of the wick created a difference in capillary pressure which replenished the wick with working fluid, hence, sustaining the flow in the loop (Gabsi, Maalej and Zaghdoudi, 2018). The vaporization of working fluid caused the local vapor pressure to increase in

the evaporator, developing a pressure differential between the evaporator section and condenser section, hence vapor phase working fluid travelled from evaporator section to the condenser section via the vapor line (Meseguer; Jose, Grande; Isabel Perez and Andres; Angel Sanz, 2012). In the condenser, the vapor loosed pressure, and condensed to liquid phase, releasing the latent heat of vaporization in the process (Zohuri, 2020). The liquid phase working fluid travelled back to the compensation chamber through the liquid line and the process repeats when heat is applied continuously.

Capillary pressure, ΔP_c, is the driving force and sustain the flow of LHP. The capillary pressure must exceed the total pressure losses in the LHP which can be calculated with the Equation 2.1 (Ambirajan et al., 2012; Gabsi, Maalej and Zaghdoudi, 2018).

$$\Delta P_C = \frac{2\sigma cos\beta}{R_P} \geq \Delta P_{ll} + \Delta P_{vl} + \Delta P_g + \Delta P_w + \Delta P_{vg} \qquad (2.1)$$

Where

ΔP_{ll} =viscous pressure drop in liquid line

ΔP_{vl} = viscous pressure drop in the vapor line

ΔP_g = the hydrostatic pressure drop

ΔP_w = the liquid pressure drop in the wick

ΔP_{vg} = the vapor pressure drop in the grooves

Equation 2.2 and 2.3 shows the formula to obtain the viscous pressure drop for liquid and vapor respectively (Gabsi, Maalej and Zaghdoudi, 2018).

$$\Delta P_{ll} = \frac{8\mu_{l,c}\dot{m}(l - l_c)}{\pi\rho_{l,c}R^4} \qquad (2.2)$$

$$\Delta P_{vl} = \frac{8\mu_{l,c}\dot{m}(l - l_c)}{\pi\left(\frac{\rho_{v,c}+\rho_{v,e}}{2}\right)R^4} \qquad (2.3)$$

Hydrostatic pressure drop is the pressure drop incurred when fluid is travelling against gravity and can be expressed by the Equation 2.4.

$$\Delta P_g = \rho_l g \Delta H \quad (2.4)$$

Liquid pressure drop in the wick can be calculated with Equation 2.5 (Gabsi, Maalej and Zaghdoudi, 2018).

$$\Delta P_w = F_w L_p Q_{in} \quad (2.5)$$

Where

$$F_w = \frac{\mu_l}{K_w A_w \Delta h_v \rho_l} \quad (2.6)$$

$$K_w = \frac{{D_P}^2 {\phi_P}^2}{150(1-\phi)^2} \quad (2.7)$$

Vapor pressure drop in the grooves and can be relate by Equation 2.8 (Gabsi, Maalej and Zaghdoudi, 2018).

$$\Delta P_{vg} = F_{vg} L_g Q_{in} \quad (2.8)$$

Where

$$F_{vg} = \frac{\mu_v}{K_g N_g A_{wg} \Delta H_v \rho_v} \quad (2.9)$$

$$K_g = \frac{{D_{hg}}^2 \phi_g}{2P_o} \quad (2.10)$$

$$\phi_g = \frac{S_g}{S_g + W_g} \quad (2.11)$$

$$P_o = 24(1 - 1.355\alpha + 1.947\alpha^2 - 1.701\alpha^3 + 0.956\alpha^4 - 0.254\alpha^5) \quad (2.12)$$

$$\alpha = \min\left(\frac{W_g}{D_g}; \frac{D_g}{W_g}\right) \quad (2.13)$$

2.3.3 Operating limits of loop heat pipe

The operation and performance of a heat pipe is heavily influenced by the shape, wick structure and working fluid. However, during steady state operation, there are five limits governing the heat transfer capabilities of a LHP which are, entrainment limit, sonic limit, boiling limit, capillary limit and viscous limit (Manimaran et al., 2019; Zohuri, 2020).

2.3.3.1 Sonic limit

At low vapor pressures, vapor velocity approached sonic speed at the exit of the evaporator (Zohuri, 2016). This caused the flow to be chocked and any further increase in pressure gradient does not increase the velocity (Sundén and Fu, 2017). Therefore, the heat transfer is limited due to the suppressed vapor flow. This phenomenon is sonic limit. Sonic limit occurred typically at start-up when circulation of working fluid caused large addition and removal of working fluid in condenser and evaporator of the heat pipe (Zohuri, 2020). Equation 2.14 is used to calculate the maximum heat flux to prevent sonic limit.

$$\dot{Q}_S = \rho_v \lambda \sqrt{\frac{\gamma R T_v}{2(\gamma + 1)}} \tag{2.14}$$

2.3.3.2 Entrainment limit

The high vapor velocity will also cause another issue which is the entrainment limit. In an ordinary heat pipe, the working fluid of different state travelled opposite to each other, meaning, liquid phase working fluid travelled from the condenser section to the evaporator section via wick while vapor phase working fluid flowed from evaporator section to the condenser section through the vapor channel (Zohuri, 2016). Shear force is exerted by the vapor working fluid on the liquid working fluid at the vapor-liquid interface (Zohuri, 2020). Liquid droplets will be entrained by the vapor flow when the shear force is larger than the surface tension of the liquid, which caused a dry-out in the evaporator section (Barbosa and Mantelli, 2021). The Weber number can be used to determine the occurrence of an entrainment. Equation 2.15 is used to calculate Weber number. To prevent entrainment the Weber number should be less than unity (Reay, Kew and McGlen, 2014a). However, entrainment limit is less relevant in LHP because of the separation of vapor and liquid line. The maximum heat flux to prevent entrainment can be calculated by Equation 2.16 (Reay, Kew and McGlen, 2014a).

$$We = \frac{2\left(r_{h,w}\right)\rho_v V_v^2}{\sigma} \tag{2.15}$$

$$\dot{Q}_E = \pi r_v^2 \sqrt{\frac{2\pi\rho_v\sigma_l}{z}} \tag{2.16}$$

2.3.3.3 Capillary limit

The capillary limit occurs when capillary pressure is insufficient to maintain the flow working fluid in the heat pipe, which caused the evaporator to experience dry-out (Zohuri, 2020). Capillary limit prevailed when the heat pipe is subjected to excessive heat load, which caused higher evaporation rate of liquid working fluid in the wick, which resulted in the inability of the capillary pressure to sustain the flow of working fluid (Sundén and Fu, 2017). Capillary limit is heavily influenced by the physical structure of the wick, and is govern by the capillary pressure drop, ΔP_c, demonstrated earlier.

2.3.3.4 Boiling limit

When heat flux is applied to the evaporator of the heat pipe, heat is transferred radially to the working fluid, hence, unlike the previous limits, boiling limit is related to radial flux constraint instead of axial flux. When sufficient heat flux is applied, formation of nucleation sites inside the wick can be observed (Barbosa and Mantelli, 2021). The bubbles formed are trapped inside the wick, which prevent heat transfer from evaporator wall to the working fluid and hindered the flow of liquid from condenser which resulted in dry-out of evaporator (Zohuri, 2020). The maximum heat flux which can be applied to heat pipe prior to nucleation is given by Equation 2.17 (Reay, Kew and McGlen, 2014a).

$$\dot{Q}_B = \left(\frac{2\pi L_e k_{eff} T_v}{\lambda\rho_v \ln\left(\frac{r_i}{r_v}\right)}\right)\left(\frac{2\sigma}{r_n} - \Delta P_c\right) \tag{2.17}$$

2.3.3.5 Viscous limit

Lastly, viscous limit occurs when the gradient of vapor pressure across the evaporator and condenser is small. Under this condition, the viscous friction dominates over inertial forces, and vapor pressure gradient is not enough to overcome the viscous forces, hence, the circulation of working fluid is restricted.

As a result, no heat is transferred. However, viscous limit is often found in cryogenic or low temperature heat pipe operations, hence, viscous limit would be less relevant in this study. Nevertheless, the design guideline would be that the vapor pressure drop should be less than 0.1 times of the vapor pressure and the maximum heat flux to prevent viscous limit is given by Equation 2.19 (Reay, Kew and McGlen, 2014a).

$$\frac{\Delta P_v}{P_v} < 0.1 \tag{2.18}$$

$$\dot{Q}_V = \frac{r_v^2 \lambda \rho_{v_e} P_{V_e}}{16 \mu_{V_e} l_{eff}} \tag{2.19}$$

The operating limits can be plotted as the function of input axial heat flux against the temperature. Combining all the operating limits of a heat pipe into one graph would generate Figure 2.8. The area under the curves shows the optimal operating range of the heat pipe.

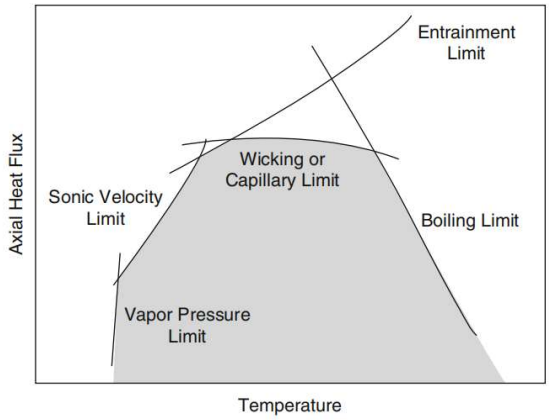

Figure 2.8: Operational Limit of LHP (Zohuri, 2020).

2.3.4 Effects of fill ratio on performance of heat pipe

Fill ratio is defined as the fraction of volume of working fluid over the whole volume of the heat pipe, and it is presented in percentage (Barba et al., 2021). A heat pipe can have a fill ratio of between 0 % to 100 %. A heat pipe is at 0% fill ratio, when it is not charged with working fluid, hence the heat transfer mode would be purely by conduction (Manimaran et al., 2019). This would result in a high thermal resistance heat pipe. At 100 % fill ratio, a heat pipe would operate

as a single phase thermosyphon (Manimaran et al., 2019). Hence, it is prominent that the fill ratio would affect the heat transfer capabilities and the operating principles of a heat pipe, while there is no definite formula to calculate the optimal fill ratio, there is a substantial number of studies done in this topic. In this section, the studies on the effect of fill ratio towards the heat transport capabilities will be reviewed.

Tharayil et al. (2016) studied the performance of LHP with varying fill ratio. Distilled water was utilized as working fluid and the filling ratios were between 20 % to 70 %. In the study, it was shown that the optimum fill ratio is around 30 %. The authors also revealed that at 30 % fill ratio and 380 W of heat load, the LHP can obtain the lowest thermal resistance of 0.106 K/W, highest value of thermal efficiency of 87 %, highest value evaporator and condenser heat transfer coefficient of 63.9 kW/m^2 and 31.8 kW/m^2 respectively. 20 % and 30 % fill ratio also reportedly have better transient start-up time among the fill ratios, demonstrating a more reliable start-up. When considering the operational limits of LHP, fill ratio of 50 % outperformed other fill ratios in terms of boiling limit, capillary limit, entrainment limit and sonic limit. The authors stated that the higher steady state operating temperature of 50 % fill ratio caused the increase in performance in term of operating limits. From the research done by the authors, it can be observed that a lower fill ratio will improve the start-up performance, while 50 % fill ratio will increase the operational limits of the LHP.

Smitka et al. (2014) performed similar experiment as Tharayil et al. (2016). However, Smitka et al. (2014) focused on fill ratio ranging from 40 % to 80 %. The results shows that the optimum fill ratio is between 60 % and 70 %, with heat removal capability of around 425 W, beyond 70 % fill ratio the LHP starts declining in heat transfer performance.

Zhang et al. (2020b) evaluated the performance of incline angle and fill ratio of three novel wickless evaporator for LHP. The LHP was charged with deionized water to the fill ratio of 30 %, 45 %, 60%, 75 % and 85 %, while the angle of inclined is $0°, 30°, 45°, 60°$ and $90°$. It was found that all three evaporators have different optimal operating ranges. However, the authors, confirmed that vertical orientation of LHP (the condenser is above evaporator), would be optimum for start-up and steady state operation. The authors also

revealed that the optimum filling ratio for all three evaporators ranges between 30 % to 60 %, as thermal resistance is the lowest within the range. The study also highlighted the difficulty of start-up for 30 %, 45 %, 75 % and 85 % fill ratio at certain inclined angles.

Reji et al. (2021) analysed the performance of thermosiphon at different fill ratio. The thermosiphon was filled with R600a as working fluid and the fill ratio range between 50 % to 70% with 10 % increments, the orientation was not varied. Results shows that 50 % fill ratio will yield the lowest thermal resistance over a range of heat input. The authors also highlighted the thermal resistance decreases with increasing heat input and stabilizes around a mean value.

Xu et al. (2018) performed similar experiment as Reji et al. (2021). However, the thermosiphon was filled with water instead of R600a. The authors focused on low fill ratio ranging from 12 % to 40 %. The results show that thermosiphon performs the best in the optimum fill ratio range of 20 % to 30 % with the thermal resistance at 0.15 °C/W. The authors concluded that at fill ratio below 20 %, dry-out in the evaporator causes the high thermal resistance, while inability of vapor to escape the liquid surface causes high thermal resistance at fill ratio above 30 %.

Rahman et al. (2016) studied the effect of orientation and fill ratio on the performance of ethanol filled pulsating heat pipe. The fill ratios between 40 % to 70 % was used in the experiment, while fill ratio below 40 % was not consider because it causes low thermal performance. They concluded that the optimum fill ratio is between 50 % to 60 % at medium heat loads (30 W-60 W), as the fill ratios provide the least thermal resistance and highest heat transfer coefficient, indicating more heat transfer. However, for low heat loads (10 W-20 W), 40 % fill ratio would be more suitable. The transient start-up time also decreases with increasing fill ratio. Lastly, the pulsating heat pipe offers the best performance when the orientation is vertical, while 45° inclined pulsating heat pipe has the fastest start-up time for all fill ratios. The research paper revealed that a heat pipe has different optimum fill ratios at different heat loads.

After completing literature review on the influence of fill ratio on the performance of heat pipe, there is no definite optimum fill ratio for all heat pipe systems. As the optimum fill ratio are dependent on various factors. For instance,

a similar heat pipe, the optimum fill ratio will be dependent on the heat load. Furthermore, the shape of the heat pipe and working fluid will also influence the optimum fill ratio. However, it can be concluded from all studies that fill ratios below 15 % will cause dry-out phenomena in the evaporator, while fill ratio of above 80 % will cause high thermal resistance hindering heat transfer. Thus, fill ratio of the heat pipe should range between 15 % to 80 %, to avoid the aforementioned problems. There will also be a trade-off between steady-state performance and start-up performance, as low fill ratio will generally provide a shorter start-up, while higher fill ratio will provide lower thermal resistance at steady-state operation. The studies also showed that heat input to the evaporator and orientation of the heat pipe will also affect the thermal resistance of a heat pipe. Through the studies, it was also revealed that vertical orientations will result in the best performance of heat pipe.

2.3.5 Modelling loop heat pipe

The heat transfer process of a LHP can be modelled thermodynamically (Maydanik, 2005; Hamdan and Elnajjar, 2009; Ambirajan et al., 2012; Reay, Kew and McGlen, 2014b; Htoo et al., 2021).

To model the LHP, eight states of the working fluid should be defined in the LHP, which can be summarized in the Table 2.4. Figure 2.9 depicts the pressure-temperature chart of the complete process of LHP.

Table 2.4: The state of working fluid and respective location in LHP.

State	Location
1	above the meniscus of the evaporator wick
2	vapor removal channel
3	entry of condenser
4	condenser
5	exit of condenser
6	entry of compensation chamber
7	inside the compensation chamber
8	inside the wick

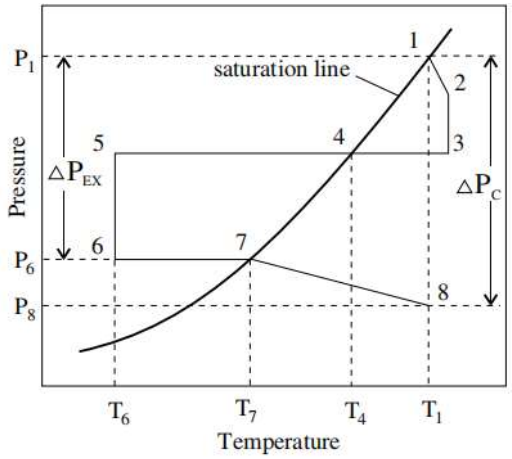

Figure 2.9: Pressure-Temperature chart of steady state LHP (Htoo et al., 2021).

Working fluid is saturated at state 1. As vapor working fluid travelled from the vapor removal chamber to the vapor line (section 1 to 2), there is a slight decreased in pressure which can be represented by ΔP_{vg}, the pressure drop also resulted in superheating of vapor. The vapor motion from vapor line to the entrance of condenser (section 2-3) is assumed to be isothermal, and the viscous pressure drop because of the vapor motion is ΔP_{vl}. Pressure losses in the condenser (section 3-5) is negligible, therefore the heat rejection occurred at constant pressure. The liquid working fluid travelled back to compensation chamber from the condenser (section 5-6) is assumed to be isothermal and the viscous pressure drop is ΔP_{ll}. The fluid inside the compensation chamber gained heat and saturated at state 7, which resulted in working fluid to exist in two phases inside the compensation chamber. Lastly, the fluid entered the wick as liquid at state 8. However, the working fluid remained liquid although the fluid is superheated, this is due to the lack of nucleation sites and the small pore size of wick, which prevented the working fluid from boiling. The thermodynamic model of LHP can be plotted into the temperature-entropy (T-S) diagram shown in Figure 2.10. The heat entered the evaporator can be determined by using Equation 2.20.

$$Q_{in} = \dot{m}(h_1 - h_6) = Q_{latent} + Q_{sensible} + Q_{leak} \qquad (2.20)$$

Where

$$Q_{latent} = \dot{m} h_{fg,e} \tag{2.21}$$

$$Q_{sensible} = \dot{m} C_l (T_{cc} - T_1) \tag{2.22}$$

$$Q_{leak} = h_{cc} A \left(T_{cc} - T_{cc,sat}\right) \tag{2.23}$$

$$T_{cc} = T_h - \left(\frac{Q - \dot{m} h_{fg,c}}{\dot{m} C_{p,l,c}}\right)\left(1 - e^{-\frac{\dot{m} C_{p,l,c} L}{k_{eff} A}}\right) \tag{2.24}$$

$$k_{eff} = k_l \varepsilon + k_s (1 - \varepsilon) \tag{2.25}$$

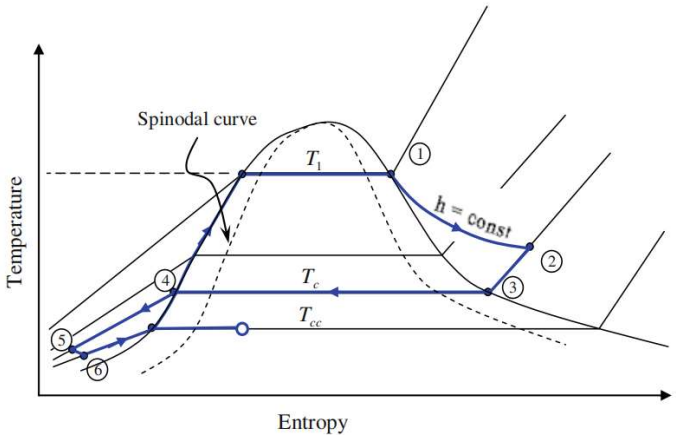

Figure 2.10: Temperature-Entropy diagram for steady state LHP (Hamdan and Elnajjar, 2009).

The heat rejection from the condenser can be calculated through Equation 2.26.

$$Q_{out} = \dot{m}(h_2 - h_5) \tag{2.26}$$

In ideal conditions the heat entered the evaporator will equal the heat rejected from the condenser.

$$Q_{in} = Q_{out} \tag{2.27}$$

$$\dot{m}(h_1 - h_6) = \dot{m}(h_2 - h_5) \tag{2.28}$$

Since the mass flow rate is the same across the whole loop

$$h_1 - h_6 = h_2 - h_5 \tag{2.29}$$

To solve Equation 2.29, thermodynamic relations need to be introduced, which are shown in Equation 2.30 to 2.34.

$$h_1 = f(T_1, P_1, x_1) \quad (2.30)$$

$$h_6 = f(T_6, P_6, x_6) \quad (2.31)$$

$$h_1 = h_2 \quad (2.32)$$

$$h_5 = h_6 \quad (2.33)$$

$$T_6 = T_{cc,sat} + \frac{Q_{leak}}{\dot{m}C_{p,l,cc,sat}} \quad (2.34)$$

2.3.6 Research on application of heat pipes in HVAC industries

There are numerous studies done on the usage of heat pipes in the HVAC industry. In this section, the aim is to review some of the studies done by researchers. Out of all the studies review, the function of heat pipe in HVAC can be classified into two categories which are energy recovery and enhancing dehumidification.

Firouzfar et al. (2012) studied the integration of heat pipe heat exchanger (HPHE) filled with silver nanofluids in air conditioning to increase the dehumidification capacity. In the paper, the authors also stated that the factors such as relative humidity, velocity and dry bulb temperature of surrounding air, filling ratio, heat pipe material and number of rows will affect the thermal performance of HPHE. The HPHE is integrated into the air conditioning system whereby the evaporator of HPHE precools the fresh air entering the air conditioner (AC), while the condenser section reheats the supply air exiting the AC. The results shows that the integration of HPHE can save up to 31.5% of energy in the AC evaporator by precooling and 100% in the reheating coil by reheating.

Abdelaziz et al. (2021) studied the ability of wickless HPHE in reducing the energy consumption of an air handling unit (AHU) type air conditioner. The authors highlighted the benefits of the HPHE being lower maintenance cost because there are no moving parts in the HPHE and avoiding cross contamination of supply air and return air in the air conditioning system. The research also studied the impact of heat pipe diameter on the performance of HPHE and concluded that heat pipe with the larger diameter will increase the

heat transfer of the HPHE. In the experiment conducted by them, the evaporator of the HPHE is installed at the fresh air duct of AHU to precool the fresh air, while condenser of HPHE is installed at the exhaust duct of the AHU. The result from the experiment shows that there are possible energy savings ranging from 28.51% to 30.85% (depending on the dry bulb temperature of incoming fresh air) compared to conventional AHU system.

Eidan et al. (2021) developed a novel heat pipe heat exchanger for window mounted air conditioner. They elaborated that the HPHE is used to improve the coefficient of performance (COP) of the vapor compression cycle of the air conditioner. The designed HPHE was a large container which contains two pairs of bended tubes, one leads refrigerant from AC evaporator to compressor and the other bring refrigerant from condenser to evaporator. The function of the HPHE is to superheat the refrigerant entering the compressor with the excess heat from the high-pressure refrigerant line. They reported that the novel HPHE improves the COP of the air conditioner by 8.42 % and 2.195 % of power savings when Acetone is used as working fluid. Figure 2.11 shows the schematic diagram of the HPHE developed by them.

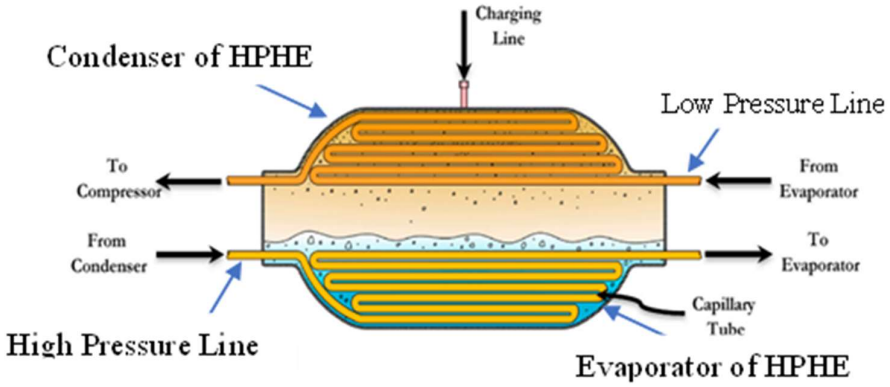

Figure 2.11: Schematic diagram of novel HPHE (Eidan et al., 2021).

Similar to Eidan et al. (2021), Nakkaew et al. (2019) developed a HPHE to enhance the efficiency of the vapor compression cycle. The HPHE has three parts which are the holder which acts as evaporator, heat pipes to transfer heat from evaporator to the cooling fins and cooling fins which is the condenser part. They installed the holder of HPHE at the outlet of the compressor of a 1 HP air conditioner. The research showed that with the integration of HPHE the

AC unit can have a 3.12 % increase in energy efficiency ratio (EER) and 3.48 % increase in COP. They concluded that the increase in performance is due to the HPHE cooling the refrigerant before the refrigerant enters the condenser, resulting in more subcooling of refrigerant at the exit of condenser, which also increase the cooling capacity of the evaporator.

Jouhara and Meskimmon (2018) investigated the feasibility of water filled wraparound heat pipes in chilled water HVAC systems to remove moisture from supply air. The evaporator section of wraparound heat pipe is used to precool the fresh air, while the condenser section is used to reheat the supply air. The experiment compares the effectiveness of water with refrigerant R134a. The effectiveness is defined as the difference in temperature across the evaporator divided by the maximum temperature difference between the air entering the evaporator and the condenser. Through the experiment, it was found that water outperformed R134a by 3.7 %.

Based on the research paper reviewed, heat pipe was integrated into an existing air conditioning system to increase the cooling performance by either energy recovery or enhancing dehumidification. However, as of now, there has not been any research conducted to investigate the usage of heat pipe as a standalone device which performs cooling function similar to an air conditioner.

2.4 Air Conditioning Process

As mentioned in Chapter 1, air conditioning in general involved four processes, cooling, heating, humidifying and dehumidifying. However, when discussing air conditioning for human comfort it usually involves the combination of cooling and dehumidifying. Hence, this section will only focus on the two processes.

The process of cooling air involved lowering the dry bulb temperature of the air, which is accomplished by passing the air through a series of coils containing refrigerant. Cooling process at constant specific humidity will increase the relative humidity of the air, causing discomfort to the user. Hence, to overcome this issue, dehumidification is performed after cooling. Dehumidification required the air to be cooled below its dew point temperature. This can be achieved by retaining the conditioned air inside the cooling section for a sufficiently long period, cooling the air to its dew point temperature. The

cooling and dehumidifying process can be illustrated in the psychometric chart as shown in Figure 2.12.

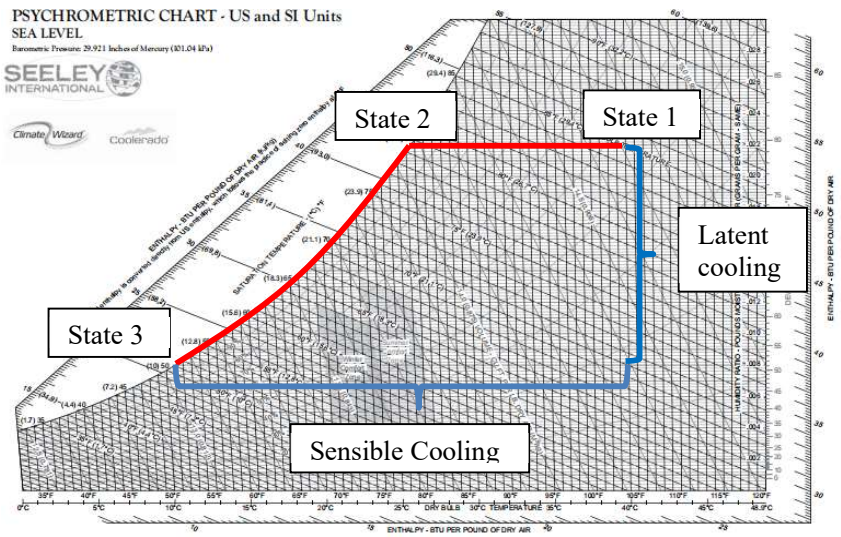

Figure 2.12: Psychometric chart for cooling and dehumidification process.

As shown in Figure 2.12, hot and humid air enters the air conditioner at state 1. The air underwent cooling at constant specific humidity from state 1 to state 2. At state 2, air is saturated and any further cooling will result in condensation of moisture. This is because at state 2, the air reached its dew point temperature and the relative humidity of the air is at 100%, which indicated that the air held the maximum amount of moisture. The air is saturated from state 2 to state 3 as moisture is removed from the conditioned air. The conditioned air is then released back to the conditioned space, where it mixed with the surrounding air, lowering both the relative humidity and dry bulb temperature of the surrounding air. From the psychometric chart, the amount of moisture and heat removed from the air also can be determined from the Equation 2.35 and 2.36.

$$\dot{m}_w = \dot{m}_a(\omega_1 - \omega_2) \tag{2.35}$$

$$\dot{Q}_{out} = \dot{m}_a(h_1 - h_3) - \dot{m}_w h_w \tag{2.36}$$

In HVAC industry, $\dot{Q}_{out}$ is referred as cooling capacity of an air conditioner which is the amount of heat removed by the system from a space

over a period of time (Subiantoro, Ooi and Junaidi, 2013). Hence, in order to determine the cooling capacity, three parameters are required, the wet and dry bulb temperature and mass flow rate of air (Rani et al., 2018). This is because with dry and wet bulb temperature, other properties such as relative humidity, enthalpy, humidity ratio can be determined through psychometric chart.

A matrix to evaluate the efficiency of an air conditioner is the Energy Efficiency Ratio (EER). EER can be obtained by dividing the cooling capacity with the electrical energy input required to achieve the cooling capacity, as shown in Equation 2.37 (Dincer and Rosen, 2013).

$$EER = \frac{Cooling\ Capacity\ [Btu/hr]}{Input\ \ Electrical\ Energy\ [W]} \tag{2.37}$$

Both the EER and COP can be used to measure the efficiency of an air conditioner, however, COP provides an instantaneous measure while EER is averaged over a period of time (Demirel, 2018). Nevertheless, star rating for efficiency of an air conditioner based on the cooling seasonal performance factor (CSPF), which can be calculated by multiplying EER by 1.062, as shown in Equation 2.38.

$$CSPF = 1.062 \times EER \tag{2.38}$$

The star rating system used by the Suruhanjaya Tenaga Malaysia can be summarized in the Table 2.5 and 2.6.

Table 2.5: Star Rating for cooling capacity below 4.5 kW (Suruhanjaya Tenaga, 2018).

Star Rating	Tested CSPF (Wh)
5	$CSPF \geq 5.30$
4	$4.60 \leq CSPF < 5.30$
3	$3.30 \leq CSPF < 4.60$
2	$3.10 \leq CSPF < 3.30$
1	$CSPF < 3.10$

Table 2.6: Star Rating for cooling capacity below 7.1 kW (Suruhanjaya Tenaga, 2018).

Star Rating	Tested CSPF (Wh)
5	$CSPF \geq 5.10$
4	$4.00 \leq CSPF < 5.10$
3	$3.10 \leq CSPF < 4.00$
2	$2.90 \leq CSPF < 3.10$
1	$CSPF < 2.90$

2.5 Thermodynamic properties of working fluid

As previously discussed in section 2.3.2, the working fluid inside a heat pipe will exist in liquid and vapor state. Thus, it is crucial to discuss the vapor pressure of a fluid as it is related to the phase change process of a working fluid. Vapor pressure can be defined as the pressure at which the gas phase of a substance is in equilibrium with the condense phase in a closed container (Speight, 2017). When the partial pressure of the working fluid's vapor molecule is less than the vapor pressure of the working fluid at a specific temperature, the working fluid will evaporate (Cengel and Bole, 2015). On the other hand, boiling occurs when temperature of the working fluid is raised above the saturated temperature at a specific vapor pressure. Equation 2.39 shows the Clausius-Clapeyron equation which is used to determine the vapor pressure of a working fluid at any given temperature. A detailed derivation of this formula can be found in the appendix.

$$P_1 = e^{\frac{\Delta H_{vap}}{R}\left(\frac{1}{T_2}-\frac{1}{T_1}\right)-lnP_2} \tag{2.39}$$

Where

$P_1 = vapor\ pressure\ at\ state\ 1$

$P_2 = vapor\ pressure\ at\ state\ 2$

$T_1 = saturated\ temperature\ at\ state\ 1$

$T_2 = saturated\ temperature\ at\ state\ 2$

$\Delta H_{vap} = latent\ heat\ of\ vaporization$

$R = Gas\ Constant$

Equation 2.39 shows that the saturated temperature of water is directly related to its vapor pressure, while the relation is not linear, in general, the saturated temperature increased along with the vapor pressure. To further illustrate, Figure 2.13 shows the graph of vapor pressure against saturated temperature for water plotted using Equation 2.39. When sufficient heat is absorbed by liquid water at saturated temperature, phase change occurs. The heat required for the phase change is termed as the latent heat of vaporization (Kirkham, 2014). At a given vapor pressure, the working fluid undergo phase changed at constant temperature which can be illustrated in Figure 2.14. For the current application, the boiling point of working fluid should fall within 25 °C to 35 °C. Hence, the corresponding vapor pressure of water would be 3.1698 kPa to 5.6291 kPa; while the corresponding vapor pressure of isopropyl alcohol would be 5.8000 kPa to 10.4000 kPa. The procedures to achieve the required conditions would be discussed in Chapter 3.

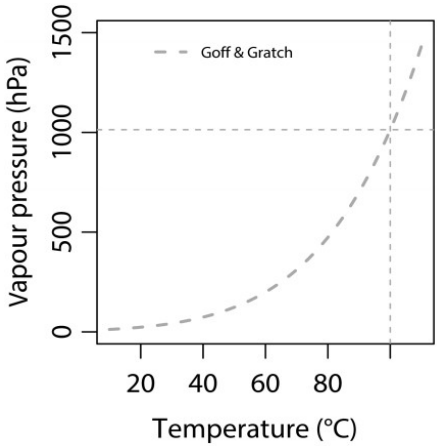

Figure 2.13: Graph of vapor pressure against temperature for water (Harrison and Marlton, 2020).

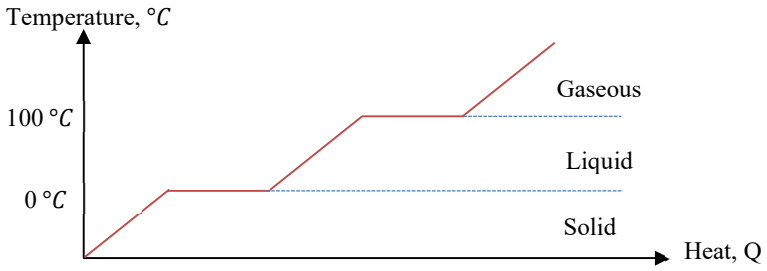

Figure 2.14: Phase change diagram for water at atmospheric pressure.

2.6 Summary

In this chapter, the importance of IEQ and thermal quality is studied. According to DOSM (2014), indoor temperature should be within the range of 24 $°C$ to 26 $°C$ and relative humidity between 50 % to 70 %. The fundamentals of LHP were also reviwed. In general, LHP has 5 components which are the evaporator, condenser, transport line, compensation chamber and wick. LHP utilised two phase flow regimes to transport heat. The five operational limits that governed the heat transport capabilities of LHP which are entrainment limit, sonic limit, boiling limit, capillary limit and viscous limit. The effect of fill ratio affects the heat transport capabilities of the LHP was also studied. However, through the study, the optimum fill ratio for LHP will be dependent on the usage, structure of the heat pipe and working fluid. Recent research for usage of heat pipes in HVAC industry was study. The applications were mostly for energy recovering purpose or enhancing dehumidification.

CHAPTER 3

METHODOLOGY AND WORKPLAN

3.1 Introduction

This chapter highlighted the methodology for this final year project. Methodology outlined the approach and procedures required to achieve the objective. The two approaches used are mathematical modelling and prototyping.

3.2 Methodology

In this study, the approach to obtain results for model validation is by constructing a prototype. Besides a mathematical modelling of the heat pipe air conditioner will also be performed to evaluate the theoretical performance of the heat pipe air conditioner. Hence, this methodology will be separated into two sections, which are the prototyping for heat pipe air conditioner and mathematical modelling of heat pipe heat exchanger. Figure 3.1 shows the flowchart for the construction of the prototype.

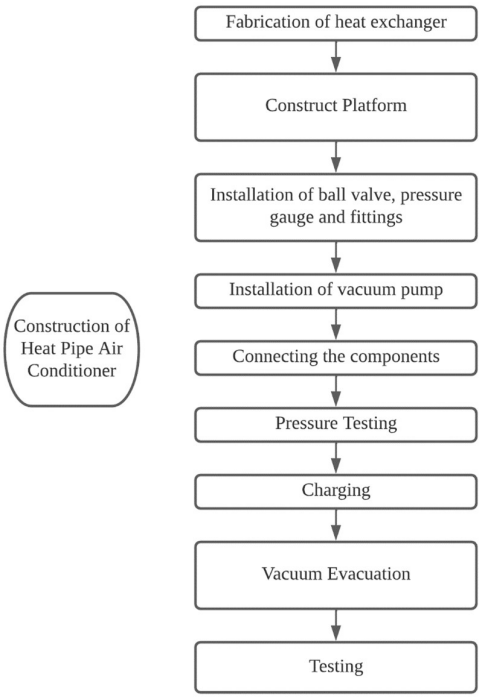

Figure 3.1: Flowchart for Heat Pipe Air Conditioner Construction.

3.2.1 Mathematical Modelling

Mathematical modelling involved theoretical calculations of the maximum heat transfer rate of the HPAC. Like a heat pipe, the working principle of a HPAC would theoretically follow the two-phase flow regime of a heat pipe, as shown in section 2.3.5. However, since the HPAC does not include a compensation chamber, the thermodynamic cycle of a HPAC can be further simplified. The pressure regulating process of the vacuum pump and ball valve are assumed to be isentropic; and no subcooling and superheating of working fluid is involved, the reversed Carnot cycle would then resemble the thermodynamic cycle of the HPAC. The T-S diagram for reverse Carnot cycle is shown in Figure 3.2, while the state points of working fluid and its represetive location can be summarised in Table 3.1.

Table 3.1: State of working fluid with its respective location.

State	Location
1	Entrance of evaporator
2	Inlet of suction side of vacuum pump
3	Entrance of condenser
4	Inlet of ball valve

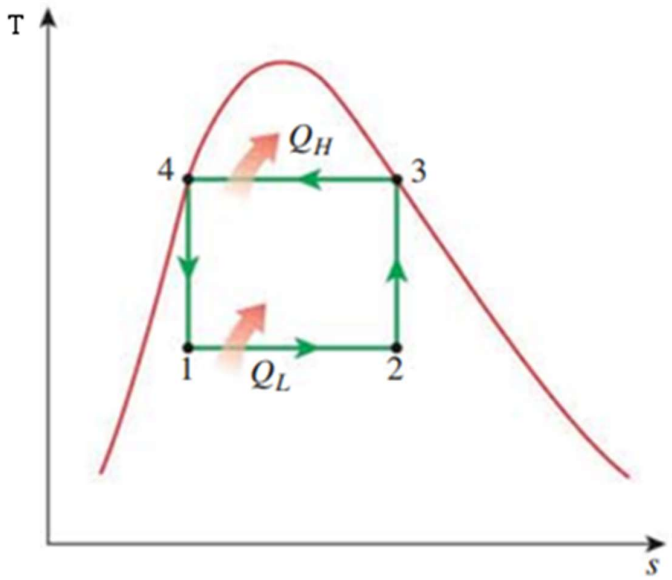

Figure 3.2: T-S diagram for HPAC (Cengel and Bole, 2015).

In ideal condition, the rate of heat entered the evaporator, $\dot{Q}_L$ would equal to the rate of heat exited the condenser, $\dot{Q}_H$, this relation can be represented in mathematical form as shown in Equation 3.1.

$$\dot{Q}_L = \dot{Q}_H \tag{3.1}$$

$\dot{Q}_L$ and $\dot{Q}_H$ can be calculated using Equation 3.2 and 3.3.

$$\dot{Q}_L = \dot{m}(h_2 - h_1) \tag{3.2}$$

$$\dot{Q}_H = \dot{m}(h_3 - h_4) \tag{3.3}$$

The thermodynamic relation for working fluid at state 3 and 4 can be defined in Equation 3.4 and 3.5 respectively.

$$h_3 = f(T_3, P_3) \tag{3.4}$$

$$h_4 = f(T_4, P_4) \tag{3.5}$$

All processes in the ideal reverse Carnot Cycle were assumed to be internally reversible, hence the entropy relation would be represented in Equation 3.6 and 3.7.

$$S_3 = S_2 \tag{3.6}$$

$$S_3 = S_2 \tag{3.7}$$

The mass flow rate of the working fluid is assumed to be the equal to the mass flow rate of the electric vacuum pump. The second law of thermodynamic defined the travel direction of energy across a boundary (Cengel and Bole, 2015). Therefore, in order for heat to flow from the ambient air to the evaporator, the evaporator temperature is required to be lower than the ambient temperature. Conversely, the condenser temperature has to be higher than the ambient temperature for heat rejection to the surroundings. In the theoretical calculations, the evaporator pressure, P_{evap}, and condenser pressure, P_{cond}, is taken to be the saturation vapor pressure of working fluid at working evaporator temperature and condenser temperature respectively. Table 3.2 shows the assumptions of the

operating parameters of the HPAC. In an ideal situation the heat entered the HPAC will be equal to the heat rejected from the HPAC. Therefore, to simplify the calculation process, the heat absorption will be calculated using Equation 3.3.

Table 3.2: Assumptions on the working conditions of HPAC.

Parameter	Value
Density of air, $\rho_{air@30°C}$	1.164 kg/m^3
Mass flow rate, $\dot{m}$	5 litre/min
Ambient Temperature, T_{amb}	$30°C$
Evaporator Temperature, T_{evap}	$25°C$
Condenser Temperature, T_{cond}	$35°C$

$$\dot{m} = 5\frac{l}{min} \times \frac{1min}{60secs} \times \frac{1m^3}{1000l} \times 1.164\frac{kg}{m^3}$$
$$\dot{m} = 9.7 \times 10^{-5}\ kg/s$$

Considering when water is used as working fluid. From Table B.13, the thermodynamic properties of water are displayed in Table 3.3.

Table 3.3: Thermodynamic properties of water.

Parameter	Value
P_{evap}	3.1698 kPa
$h_{f@3.1698\ kPa}$	104.83 kJ/kg
$h_{g@3.1698\ kPa}$	2546.5 kJ/kg
P_{cond}	5.6291 kPa
$h_{f@5.6291\ kPa}$	146.64 kJ/kg
$h_{g@5.6291kPa}$	2564.6 kJ/kg

$$\dot{Q}_H = (9.7 \times 10^{-5})(2564.6 - 146.64)$$
$$\dot{Q}_H = 0.235\ kJ/s$$

Now, the scenario when isopropyl alcohol is used as working fluid is considered. From Table B.14, the thermodynamic properties of isopropyl alcohol are displayed in Table 3.4.

Table 3.4: Thermodynamic properties of isopropyl alcohol.

Parameter	Value
P_{evap}	5.8000 kPa
$h_{f@5.8\ kPa}$	260.91 kJ/kg
$h_{g@5.8\ kPa}$	1017.7 kJ/kg
P_{cond}	10.4000 kPa
$h_{f@5.6291\ kPa}$	287.75 kJ/kg
$h_{g@5.6291kPa}$	1032.3 kJ/kg

$$\dot{Q}_H = (9.7 \times 10^{-5})(1032.3 - 287.75)$$
$$\dot{Q}_H = 0.072\ kJ/s$$

Both of the theoretical calculation showed that the concept of HPAC is feasible. The mathematical modelling shows that when the evaporator pressure and condenser pressure were manipulated to the saturated vapor pressure of the working fluid at the corresponding ambient temperature, heat transfer will occur.

3.2.2 Prototyping

To construct the prototype, 4 main components are required. The components and its function can be summarised in Table 3.5.

Table 3.5: Components of Heat Pipe Air Conditioner and its function.

Component	Function
Heat Exchanger	To absorb heat from the conditioned space To expel heat to the environment
Electric Pump	To reduce pressure inside the evaporator
Ball Valve	To regulate the pressure inside the evaporator
Polyurethane Pipes	To transport working fluid between the two components evaporator and condenser

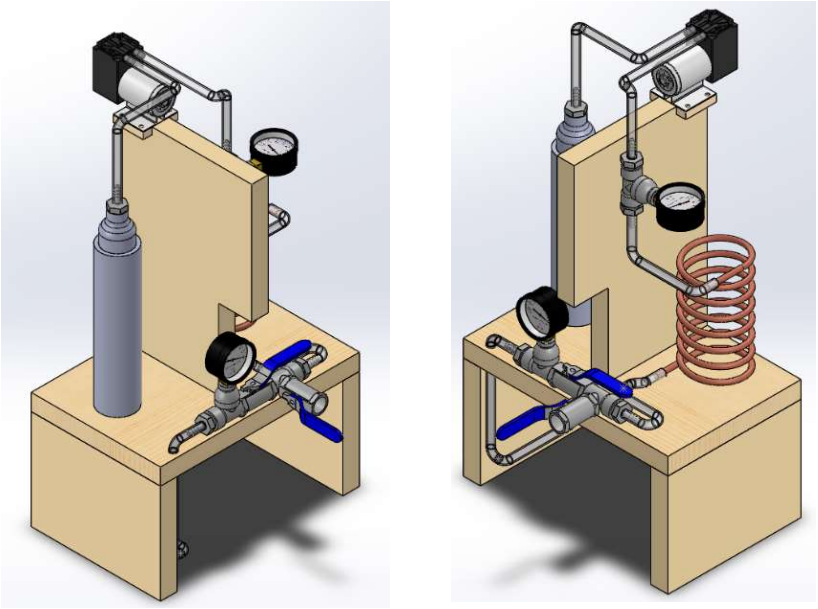

Figure 3.3: 3D modelling of prototype.

Figure 3.3 shows the 3D modelling of the prototype, which was used as a guide for the construction of prototype. To construct the heat pipe air conditioner prototype, there are 10 steps which will be discussed below.

3.2.2.1 Fabrication of heat exchangers

The condenser side heat exchanger was fabricated using copper tubes. The copper tube selected has an outer diameter of 6.35 mm and wall thickness of 0.51 mm. To fabricate the helical coils, the copper tubes were cut into 2 m section. Then, one of the ends were crimped using pliers. Salt was used to fill in the void inside the copper tube to prevent kinks in the walls of copper tube during bending process. After the copper tube was fully filled, the open end of the copper tube was crimped. To obtain the helical shape, the copper tube was wrapped around a cylindrical can to form it. Subsequently, the coiled copper tube was removed from the cylindrical can and the crimped ends were cut off using a pipe cutter. Lastly, the coiled copper tubes were immersed in water to remove the salt. Figure 3.4 shows the fabricated helical coil copper tube.

Initially, helical coil copper tube was also used as the evaporator of the prototype. However, after preliminary testing, it was found that modification in terms of its structure to the evaporator is necessary for the prototype to function properly. A detailed explanation of the problems faced by the helical coil copper

tube as an evaporator can be found in the appendix. The evaporator side heat exchanger is fabricated from a 2-inch galvanised iron (GI) pipe. The inside of the pipe is thoroughly cleaned with paint thinner to remove oil contaminants and rinsed with water and soap. Due to the lack of proper sized sockets, both ends of the GI pipe is forged to ensure the sockets will meet up with openings of the GI pipe. The galvanised layer on the GI pipe was removed with an angle grinder in order to prepare the mating surfaces for welding. Then two 1-inch to 1/2-inch galvanised iron sockets were welded onto both ends of the GI pipe as shown in Figure 3.5. Then two 1/2-inch barb fittings were fitted onto the sockets in preparation of assembly.

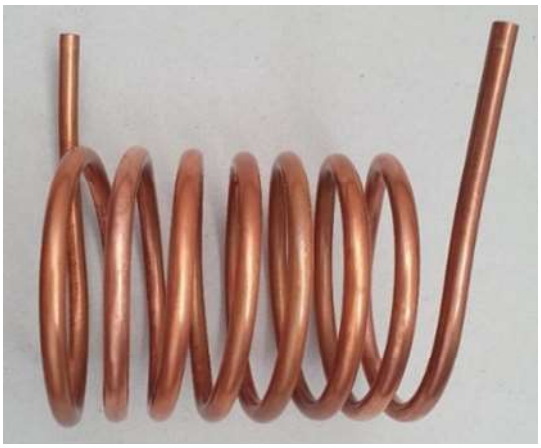

Figure 3.4: Helical coil copper tube.

Figure 3.5: GI pipe with welded GI sockets.

3.2.2.2 Platform Construction

The platform will act as a backbone for the components to be mounted onto. The platform was constructed with wood. The dimensions of the platform were displayed in Figure C.1, C.2 and C.3 (Appendix C). To secure the three separate pieces, screws and L-brackets were used.

3.2.2.3 Installation of ball valve, pressure gauge and fittings

The fittings were thoroughly inspected for defects. Next, the male threads of the fittings and pressure gauges were wrapped with Teflon tape. Teflon tape is used to provide a layer of sealant and prevent leakages of working fluid from the system to the surroundings. The fittings were joint together at the appropriate location, as shown in Figure 3.6. The assembled fittings, ball valve and pressure gauge were mounted onto the platform with pipe clamps as shown in Figure 3.7.

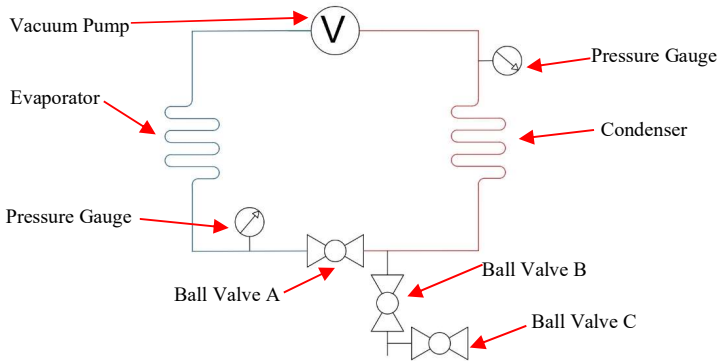

Figure 3.6: Schematic diagram of the prototype .

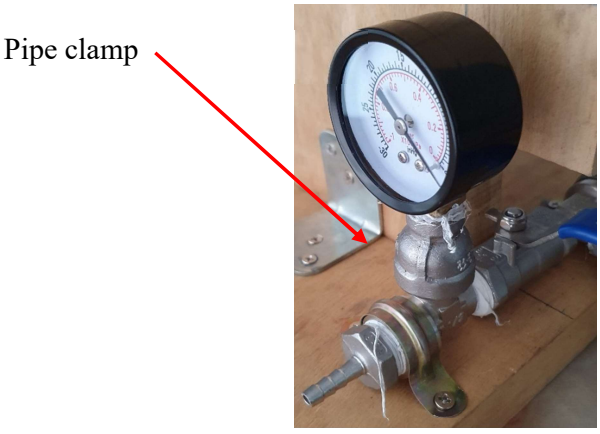

Figure 3.7: Example of installation of fitting, ball valve and pressure gauge using pipe clamps.

3.2.2.4 Installation of vacuum pump

The vacuum pump was placed and secured onto the platform with screws. The suction side of the vacuum pump should be connected to the evaporator while the discharge side is connected to the vapor line. The vacuum pump specification of the vacuum pump can be summarized in Table 3.6. The vacuum pump used in the prototype is shown in Figure 3.8.

Table 3.6: Specification of vacuum pump.

Parameter	Specification
Voltage	12 V (DC)
Current	0.5 Amp
Volumetric Flow Rate	5 l/min
Suction Pressure	65 kPa

Figure 3.8: Picture of vacuum pump.

3.2.2.5 Connecting the components

The ball valve, vacuum pump, heat exchanger and fittings are connected using polyurethane hose. Polyurethane hoses are cut to the appropriate length prior to installation. To ensure the connection between the polyurethane hose and the components were secure, wire clamps were used. In addition to wire clamp, silicone sealant was used at the joints to provide extra layer of sealing. The completed prototype is showed in Figure 3.9.

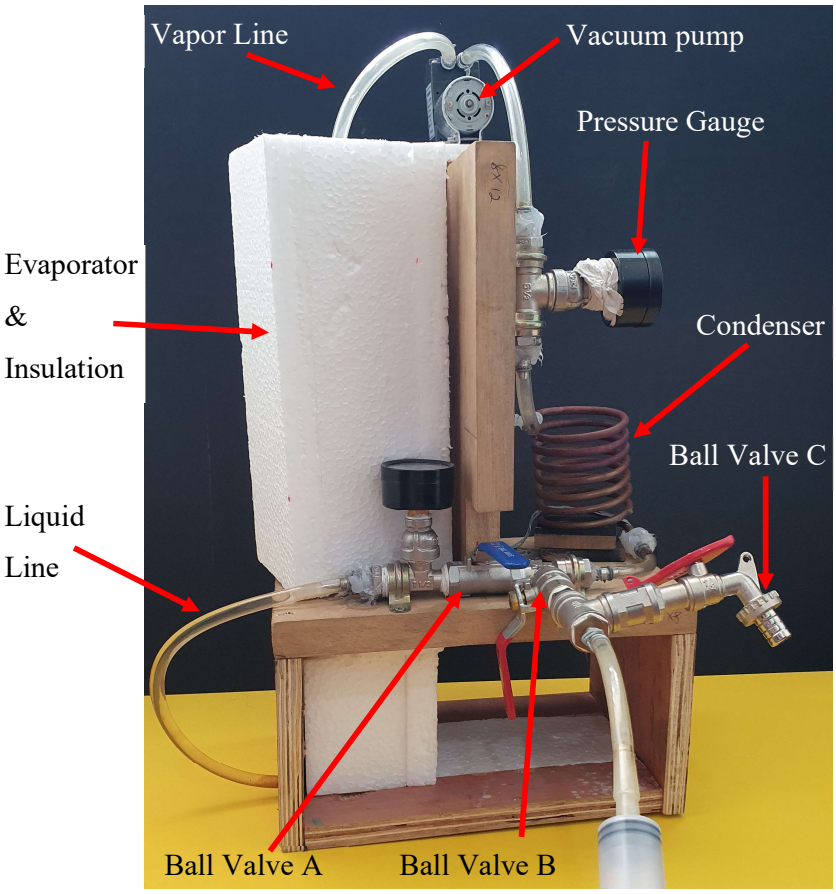

Figure 3.9: Fully assembled prototype.

3.2.2.6 Pressure Testing

The completed prototype is then subjected to pressure testing. To perform pressure testing additional fittings were installed as shown in Figure 3.10.

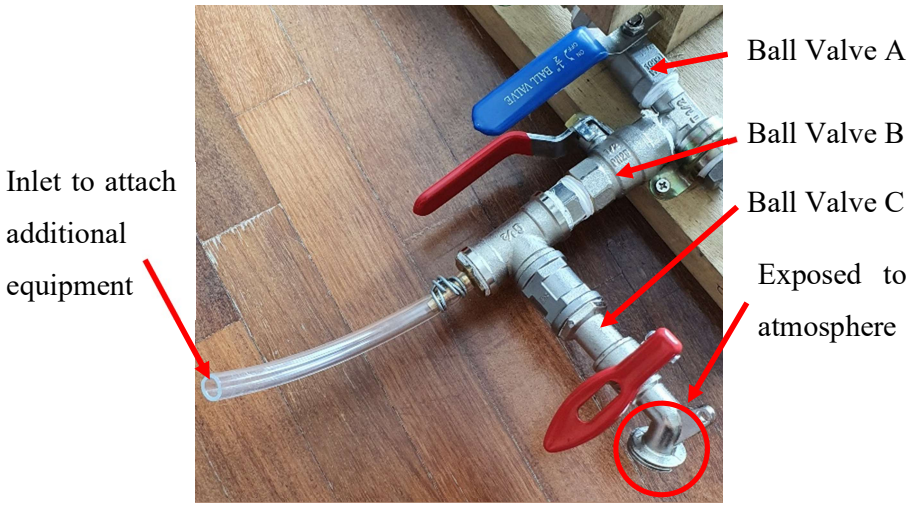

Figure 3.10: Pressure testing fittings.

There are two pressure tests to be carried out, negative pressure test and positive pressure test. To carry out the negative pressure test, a syringe is attached to the inlet of polyurethane hose. First, ball valve C is opened, the syringe is compressed to empty the air content inside it. Next, ball valve C is closed, and ball valve B is opened. The syringe is extended to draw a vacuum inside the system. Ball valve B is then closed, and the process was repeated until the reading on the pressure gauges show -50 kPa. The system would be left in the partial vacuum state to be observe for any leakage in the system. The system should pass the leak test if the pressure does not have huge increment in pressure in 5 minutes.

If the system does not pass the negative pressure test, a positive pressure test will be carried out to determine the source of leakage. First, ball valve B is opened while ball valve C is closed. A positive pressure is introduced into the system through the polyurethane hose; In the case of this experiment, the source of positive pressure is a pneumatic pressure hose. While the system is under positive pressure, soapy water is sprayed onto the joints and observation were made for bubbles. Bubbles were an indication of leakage. Hence, the faulty joint was redone to ensure there is no leaking.

3.2.2.7 Selection of Working Fluids

In this experiment, tap water and 99.9 % isopropyl alcohol were selected as working fluid. Two working fluids were used to examine the effects of vapor pressure on the cooling performance. Extensive studies have summarized the working fluid used in heat pipes and its corresponding range of operating temperature. Among the working fluids, acetone, methanol, Flutec PP2, ethanol, heptane was suitable for this experiment as the operating temperature of the prototype in this experiment fell within those of the working fluids (Wallin, 2012; Zohuri, 2016). However, isopropyl alcohol and tap water were selected as the working fluid because, both fluids are easily accessible and have different vapor pressures at room temperature (30°C), thus allowing the effect of vapor pressure to be studied.

3.2.2.8 Charging

The purpose of charging is to fill the prototype with working fluid. A syringe filled with the working fluid was attached to the inlet of the prototype as depicted in Figure 3.10. Ball valve C is closed, while ball valve A and B are opened. The prototype is tilted towards the evaporator side, to allow the working fluid to fill the evaporator only. The syringe is compressed, and valve A and B is closed. The process is repeated for four times each with 50 ml of working fluid. After the fourth filling, to ensure there are no fluids left in the fittings and piping, a positive pressure is introduced into the prototype. This is done by ensuring ball valve A and B were closed, while ball valve C is opened. The syringe is pull to its extended position. Ball valve C is then closed, and ball valve A and B is opened. The syringe is compressed to introduce pressure into the prototype, all while keeping the prototype in the tilted position. This is repeated for a few times, until there is no fluid drained from the fittings as shown in Figure 3.11.

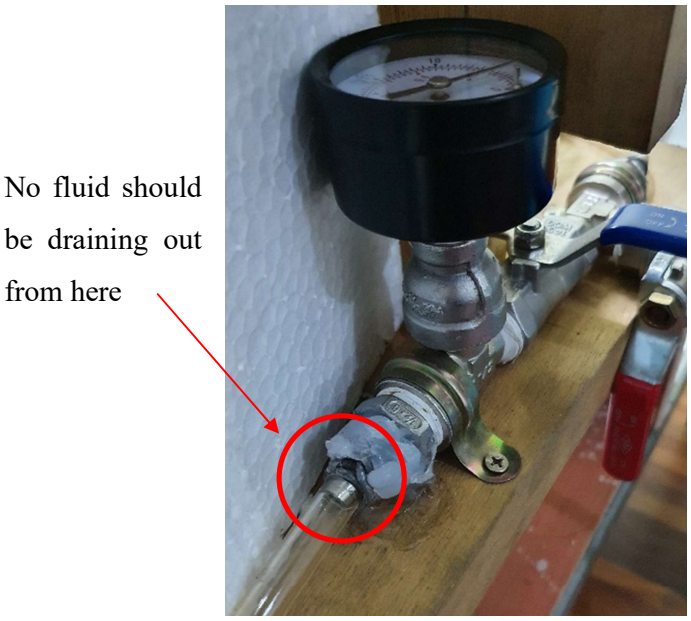

Figure 3.11: Exit of fitting towards evaporator.

3.2.2.9 Vacuum Evacuation

In vacuum evacuation, the goal is to lower the pressure inside the heat pipe air conditioner to the operating pressure of the system. To perform vacuum evacuation, a syringe is attached to the inlet to the prototype illustrated in Figure

3.10. The syringe should be in the fully compressed position before vacuum evacuation. All ball valves are closed. The syringe is extended, and ball valve B is opened; hence vacuum is drawn from the system. Ball valve B is then closed, while ball valve C is open. The syringe is then compressed, and ball valve C is closed. The process is repeated until the desired pressure is reached.

3.3 Experiment

After the prototype is completed and preparation works in terms of charging and vacuum evacuation were performed. The prototype was ready to undergo experimentation. The experiment begins with testing followed by data processing which will be further elaborated in the following section.

3.3.1 Testing

To begin testing, ball valve A is throttled. This is done to allow the flow of working fluid from the helical coil copper tube condenser to the GI pipe evaporator, while providing a pressure gradient between the evaporator and condenser. The handle position of ball valve A is marked to ensure the ball valve handle is returned to the same position. The pump is then turned on. One of the objectives were to evaluate the performance of the heat pipe air conditioner. To validate the concept, the temperature difference between the evaporator and atmosphere will be taken as a sign of the functioning of the prototype. The temperature of the evaporator, condenser and surrounding temperature will be taken using a food thermometer. The tip of the probe illustrated in Figure 3.12 is made in contact with the evaporator and condenser as shown in Figure 3.13. After the temperature stops altering, the reading was taken. The temperatures are taken at the start of the test and at 20 minutes intervals until 60 minutes is reached. The reason for the test to terminate after 60 minutes is because, after the preliminary testing, it was found that the temperature does not alter after running the prototype for 80 minutes, hence it was assumed that the prototype has reached its steady state at 60 minutes. The experiment was carried out in 6 different working pressure which is 26 kPa, 30 kPa, 40 kPa, 60 kPa, 80 kPa and 100 kPa (absolute pressure). The whole experiment was performed twice using tap water and 99.9 % isopropyl alcohol separately as working fluid.

Figure 3.12: Food Thermometer.

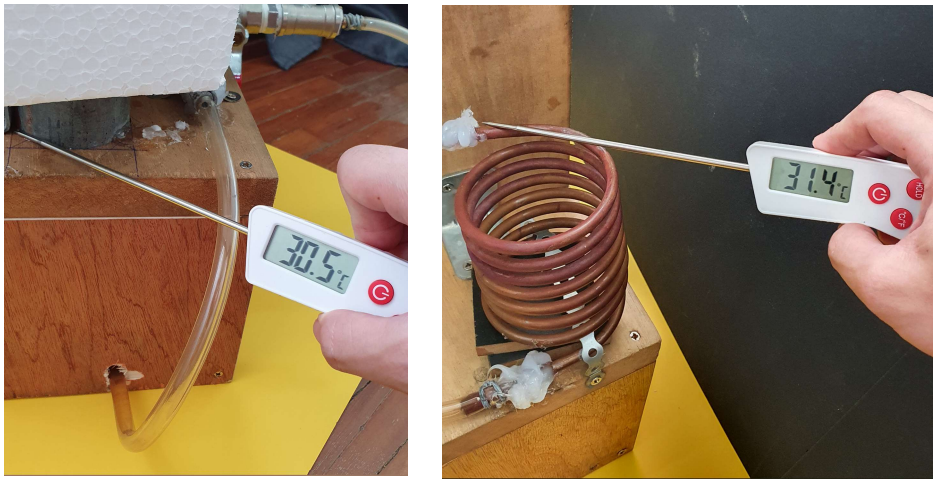

Figure 3.13: Examples of collection of data using food thermometer.

3.3.2 Data Processing

The collected data is then tabulated in a table form shown in Table B.1 to B.12. Temperature difference, ΔT can be calculated using Equation 3.8. Temperature difference is the driving force for heat transfer. As the difference in temperature increases, the rate of heat transfer will increase (Cengel and Ghajar, 2020). Thus, the ΔT over will be used as an indicator for the cooling performance of the prototype. As the ΔT over time increases, rate of heat transfer will also increase, thus cooling performance will increase.

$$\Delta T = T_{amb} - T_{evap} \tag{3.8}$$

Where

$T_{amb} = ambient\ temperature$

$T_{evap} = evaporator\ temperature$

Once the temperature difference is calculated for all datapoints, the graph of ΔT over time for various evaporator pressure and ΔT_{max} over evaporator pressure

can be plotted. The graphs are plotted using Microsoft Excel for both tap water and 99.9 % isopropyl alcohol.

3.4 Summary

In this chapter, the two approaches to obtain data was discussed. mathematical modelling and prototyping were considered as a mean to acquire the results. In the mathematical modelling of HPAC, it is found that when the evaporator and condenser pressure are adjusted to the appropriate vapor pressure in relation to the surrounding temperature, heat transfer will occur. In this chapter, the methods to construct the prototype and procedure to perform the experiment were also discussed.

CHAPTER 4

RESULTS AND DISCUSSION

4.1 Introduction

This chapter focused on the results obtained from the experiment and discussion on the results obtained. In the first subchapter, the data were displayed in graphical form, the detailed data from the experiment were displayed in the appendix. In the latter part of this chapter, discussions on the operating principle of the prototype and factors affecting the heat transfer rate were made.

4.2 Results

In this test, the two working fluids used are 99.8% isopropyl alcohol and tap water. As mentioned in section 3.2.2.9, the temperature of the evaporator, condenser and ambient air was recorded at a 20-minute interval for 60 minutes. The graph of ΔT against time was plotted. In addition to that, the graph of ΔT_{max} against evaporator pressure was also plotted. Also mentioned in section 3.2.2.10, temperature difference between evaporator and ambient air (ΔT) will be taken as an indication of the functioning of prototype. In layman terms, ΔT can be viewed as the cooling performance of the prototype. Figure 4.1 and 4.3 shows the ΔT against time for various evaporator pressure. For a working prototype, significant increase in ΔT over time should be observed. Figure 4.2 and 4.4 shows the ΔT_{max} against evaporator pressure. These graphs will show the evaporator pressure which provides maximum cooling performance. The evaporator pressure refers to the absolute pressure inside the evaporator chamber.

Where

$$\Delta T = T_{amb} - T_{evap} \quad (4.1)$$

$$\Delta T_{max} = \max\left(T_{amb} - T_{evap}\right) \quad (4.2)$$

$T_{amb} = ambient\ temperature$

$T_{evap} = evaporator\ temperature$

4.2.1 Tap Water

In Figure 4.1, the ΔT over time tend to take on a more horizontal line, indicating that there is lesser change in temperature. When evaporator pressure is at 26 kPa, ΔT increased 0.1 °C over 60 minutes. As the evaporator pressure increased to 30 kPa, ΔT increased slightly from 0.8 °C to 0.9 °C before decreased to 0.6 °C at 60 minutes. At evaporator pressure of 40 kPa and 60 kPa followed the pattern of that at 30 kPa, while at 80 kPa the ΔT fluctuated between -0.1 °C to 0.1 °C. At evaporator pressure of 100 kPa, the largest increment of ΔT was recorded at 0.7 °C from 0 minute to 20 minutes.

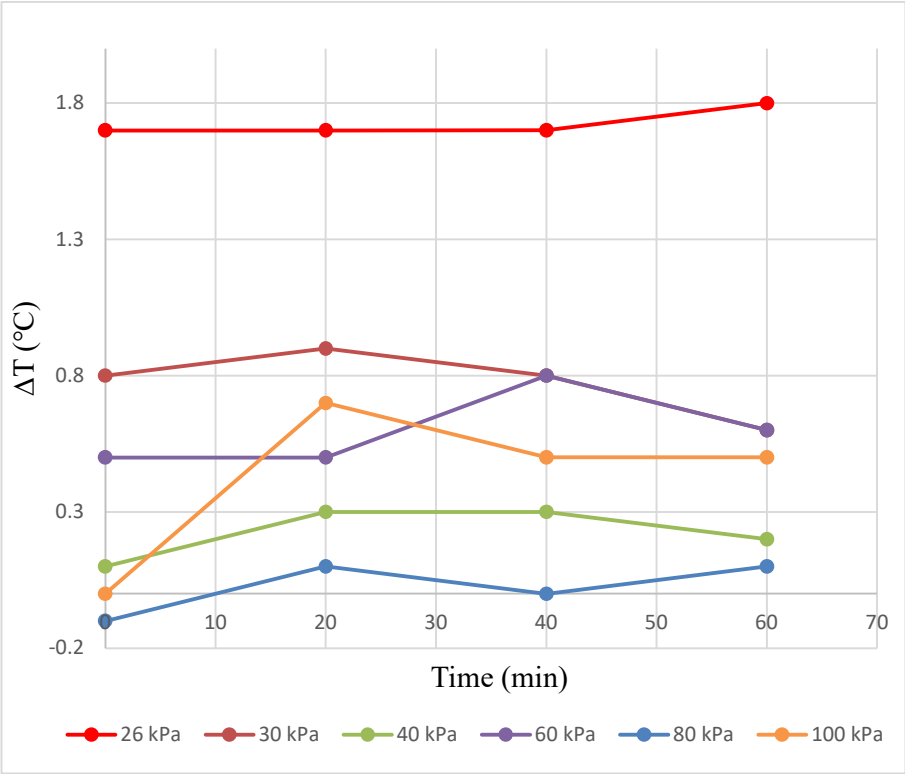

Figure 4.1: Graph of ΔT against time for various working pressure.

Based on Figure 4.2, the largest ΔT_{max} was recorded at 1.8 °C, when the evaporator pressure is 26 kPa. The ΔT_{max} decreases as the evaporator pressure increased from 26 kPa to 40 kPa. From 40 kPa to 60 kPa, ΔT_{max} increased slightly before decreased to the lowest at 80 kPa; and increased again when evaporator pressure increases from 80 kPa to 100 kPa.

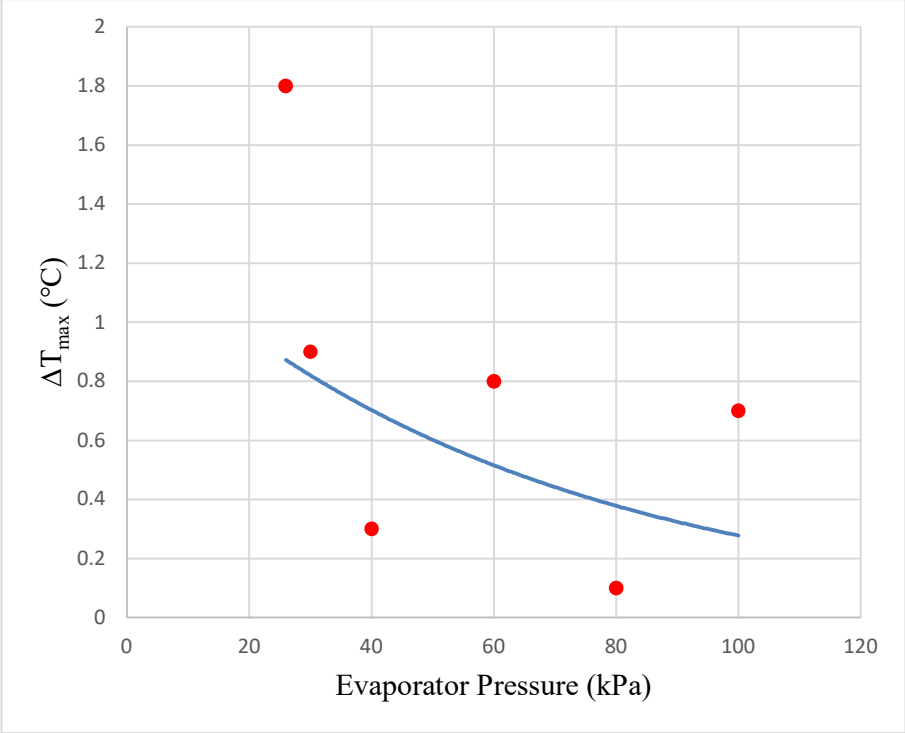

Figure 4.2: Graph of ΔT_{max} against evaporator pressure.

It can be observed that, when tap water is used as working fluid, there is no clear trends in the varying evaporator pressure and the ΔT. Both of the graphs also showed inconsistent indications. This is because, Figure 4.2 shows ΔT_{max} was the highest at evaporator pressure of 26 kPa, which indicated the highest cooling performance. However, based on Figure 4.1, there is no significant increase in ΔT over time, suggesting that there is no cooling in the evaporator. This result was not expected, as the prototype should perform better cooling at lower evaporator pressure, indicating that, at lower evaporator pressure, there should be a larger increment of ΔT. As the evaporator pressure increased, the increment of ΔT should decrease.

From the result obtained, when tap water is used as working fluid, for all evaporator pressures, there is no cooling performed as the initial ΔT is closed to the final ΔT, implying that the prototype provided almost no cooling due to the small increment of ΔT over time. Moreover, the fluctuations in ΔT over time observed in Figure 4.1 are caused by the changed in surrounding temperature. From Table B.7 to B.12, the initial temperature of the evaporator, condenser and surrounding temperature were not constant, this indicated that the initial

conditions of the prototype varied for different evaporator pressures, therefore, the initial starting points (Time = 0 minutes) in Figure 4.1 is different for all evaporator pressures. Furthermore, data in Table B.7, B.8, B.11 and B.12, revealed that the evaporator temperature increased over time, which further proved that the prototype did not perform cooling. The increase in evaporator temperature maybe caused by the increased in surrounding temperature. When the temperature of the evaporator remains constant, as shown in Table B.9 and B.10, it can be observed that the surrounding temperature fluctuates. Therefore, it can be observed that the surrounding temperature and initial conditions of the prototype will lead to inaccurate results, which translate to the fluctuation in ΔT observed in Figure 4.1. The reason tap water did not perform cooling maybe due to its inability to evaporate, which will be explored further in section 4.3.

4.2.2 Isopropyl Alcohol

From Figure 4.3, when the evaporator pressure is the range of 26 kPa to 60 kPa, there is a significant increase in ΔT over time. At evaporator pressure of 80 kPa there is a decrease in ΔT over time. Lastly, at 100 kPa, there is a slight increase in ΔT over time. Another observation that can be made from Figure 4.3, the largest increment of ΔT from 0.8°C to 2.5°C is at evaporator pressure of 26 kPa. As the evaporator pressure increased from 26 kPa to 60 kPa, the increment of ΔT over time decreased. From the results obtained, although at 100 kPa evaporator pressure, there is a slight increase in ΔT. However, the increase in ΔT was caused by the increase in surrounding air temperature. In fact, observing the data which can be found in Table B.6, the evaporator temperature remained constant at 29.1 °C, which suggested that the prototype cannot perform cooling at 100 kPa. Similarly, at evaporator temperature 80 kPa, the decreased in ΔT over time is caused by the fluctuation in surrounding temperature, while evaporator temperature remained constant at 29.8 °C, again suggesting that there is no cooling effect. From Figure 4.3, it can also be observed that at 20 minutes, the ΔT of 26 kPa (evaporator pressure) is lower than that of 30 kPa, 40 kPa and 60 kPa (evaporator pressure), although at 26 kPa (evaporator pressure) the initial ΔT is higher than the other evaporator pressures. This is due to the decreased in surrounding temperature when the experiment was carried out at evaporator pressure of 26 kPa, which can be observed in Table B.1. The

decrease in the surrounding temperature will adversely reduce the ΔT. Conversely, from Table B.2 to B.4, when surrounding temperature increased, the ΔT will increase. Thus, it can be observed that an increased in surrounding temperature will further contribute to enhance the cooling performance. Therefore, as previously discussed, the surrounding temperature will significantly impact the results. However, at evaporator pressure 60 kPa and below, despite fluctuation in surrounding temperature, the data shows that there is a significant increase in temperature difference, suggesting that the prototype had performed cooling. In addition to that, the evaporator experienced significant decrease in temperature over time, further proved the functioning of prototype.

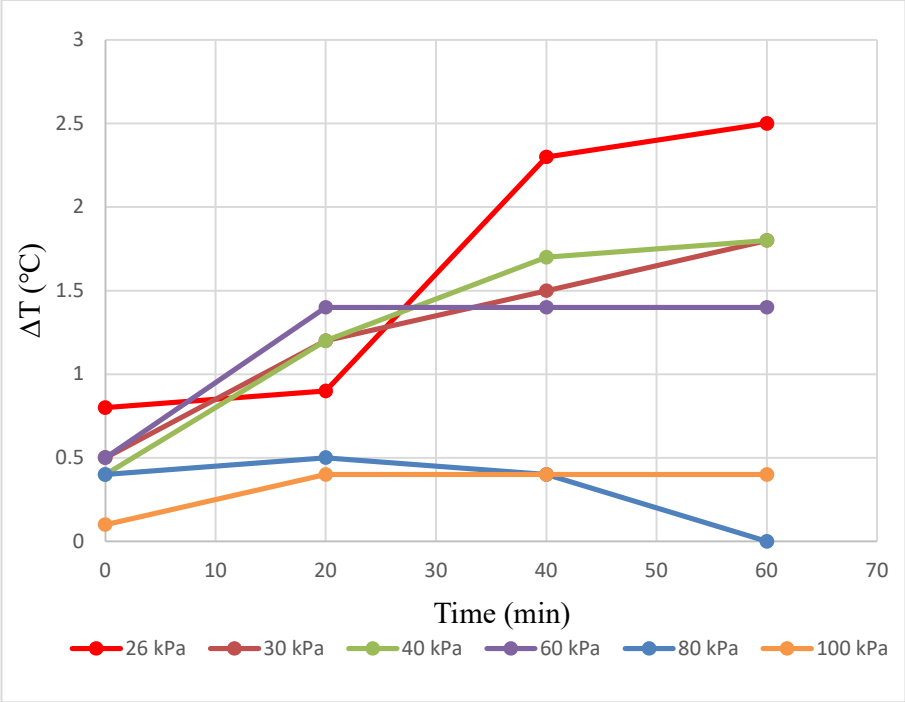

Figure 4.3: Graph of ΔT against time for various working pressure.

Referring to Figure 4.4, the graph shows a downtrend in ΔT_{max} when the evaporator pressure increased from 26 kPa to 100 kPa. The highest maximum temperature differential was recorded at 2.5 °C when evaporator pressure is 26 kPa, while the lowest maximum temperature differential was recorded at 0.4 °C. Figure 4.4 shows at evaporator pressure of 26 kPa, the prototype performed the most cooling. Coincidentally, at that pressure, the

evaporator temperature also decreased by the same amount, which is the highest among the other evaporator pressures. The results obtained when isopropyl alcohol is highly favourable to prove the concept of heat pipe air conditioner. This is because the results showed huge increment of ΔT over time for lower evaporator pressure (26 kPa to 60 kPa), while the evaporator temperature also decreased over time. The ΔT_{max} also increased as pressure decreased, which further strengthen the theory. The results shown is related to the diffusion coefficient and the vapor pressure of the working fluid which will be further explained in section 4.3.

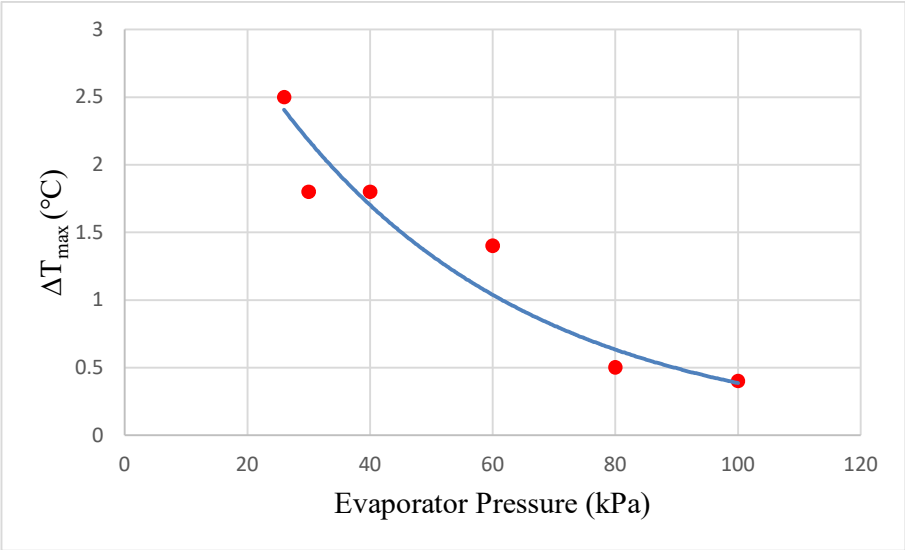

Figure 4.4: Graph of ΔT_{max} against evaporator pressure.

4.3 Overall Discussion

4.3.1 The working principle of heat pipe air conditioner

Based on section 4.2.2, the theory of HPAC can be validated. This is because large ΔT over time is observed at low evaporator pressure (26 kPa to 60 kPa). This shows that the prototype had performed cooling. Hence, in this subchapter, the theory behind the operation of the heat pipe air conditioner is discussed.

The working principle of a heat pipe air conditioner will be similar to a typical LHP. However, HPAC differs structurally when compared to a LHP. To begin with, capillary pressure was generated by the wick structure to transport the working fluid (Zhang et al., 2021). However, instead of a wick structure the HPAC has an electric vacuum pump, which provides the driving

force in terms of suction pressure. The heat pipe air conditioner also has a ball valve which separates the evaporator and condenser, providing a pressure differential between the two components. The heat pipe air conditioner consisted of five components which are evaporator, vacuum pump, condenser, ball valve and transport lines. The arrangement and connections of the components are illustrated in the schematic diagram shown in Figure 3.6.

During start-up of the prototype, all of the liquid working fluid are located in the evaporator, and no working fluid is present in the condenser. Assuming that during initial state, the heat transfer from the surroundings is small, liquid phase working fluid inside the evaporator will evaporate into vapor phase until the equilibrium phase is reached, which indicated that condensation rate is equal to evaporation rate (Speight, 2020). At equilibrium state, the vapor molecules will exert a partial pressure on the liquid working fluid and walls of the evaporator chamber; the partial pressure is termed as the saturated vapor pressure of the working fluid (Bokoch and Weston, 2020).

Dalton's law of partial pressure which states that, under a fixed volume and temperature system, the summation of partial pressure of individual gas would be the equivalent of the pressure of mixture of gases in the same volume and temperature (Sforza, 2017; Speight, 2017). In this experiment, the total evaporator pressure, P_{evap}, would be the summation of partial pressure of gasses present in the evaporator chamber and the partial pressure of the vapor working fluid, this can be displayed in mathematically as shown in Equation 4.3. The partial pressure of the individual components can be express as a function of mass (m), volume (V), gas constant (R) and temperature (T), shown in Equation 4.4.

$$P_{evap} = P_{N_2} + P_{O_2} + P_{wf} + P_m \tag{4.3}$$

Where

$P_{N_2} = partial\ pressure\ of\ nitrogegn$

$P_{O_2} = partial\ pressure\ of\ oxygen$

$P_{wf} = partial\ pressure\ of\ vapor\ \ working\ \ fluid$

$P_m = partial\ pressure\ of\ miscellaneous\ gasses$

$$P = \frac{m}{V} RT \tag{4.4}$$

Since the prototype is a closed system, the concentration of the gases, gas constants, volume will remain constant. As the temperature of gasses in the evaporator will not vary significantly during lowering of pressure, hence the temperature of gasses is assumed to be constant (Jin, 2007). Thus, the partial pressure would only depend on the mass of the gas and vapor. When the vacuum pump is switched on gases and vapor present in the evaporator is being removed from the evaporator, resulting in the decreased of evaporator pressure (Bavishi and Raiyani, 2017). According to Dalton's law of partial pressure, the partial pressure of the vapor working fluid will decrease along with the decreased in total pressure (Holloway and Pritchard, 2017). At this state, the partial pressure is lower than the saturated vapor pressure of the working fluid. Hence, to maintain equilibrium, the liquid working fluid will continuously evaporate, until the rate of evaporation equals to the rate of condensation. However, due to the continuous operation of the vacuum pump, the state of equilibrium cannot be achieved and working fluid will continuously evaporate.

During transient state, the rate of evaporation is faster than the rate of condensation. This driving force is caused by the difference in the vapor pressure and partial pressure of the working fluid induced by the vacuum pump (Cengel and Bole, 2015). As the liquid working fluid transformed its phase to vapor, it absorbed the latent heat of vaporization from the liquid phase working fluid (Liberty et al., 2013). This caused the temperature of liquid phase working fluid to decrease. As the temperature of liquid working fluid decreased below the atmospheric temperature, heat from the surrounding air entered the evaporator and transferred to the liquid working fluid. Therefore, providing cooling in the vicinity of the evaporator. The vapor then travelled through the vacuum pump and then discharged into the condenser. In the condenser, the partial pressure of the vapor working fluid is higher than the vapor pressure, thus, the vapor working fluid condensed, in the process, released heat in the form of latent heat of vaporization. Figure 4.5 captured the condensates forming in the transport line connecting the vacuum pump to condenser, during the

operation of the prototype. The liquid phase working fluid then travelled through the ball valve and re-entered the evaporator as liquid working fluid.

Figure 4.5: Condensate forming in transport line heading towards condenser.

4.3.2 Factors affecting the heat transfer rate

In the experiment, two types of fluid were used as working fluid, which are 99 % isopropyl alcohol and water. In general, when isopropyl alcohol is used as working fluid, the cooling performance of the prototype is better than tap water. In the experiment, the evaporator pressure was also manipulated to observe the cooling performance of the prototype in relation to the evaporator pressure. Based on the results obtained, when isopropyl alcohol is used as working fluid, at lower evaporator pressures, from 26 kPa to 60 kPa, the prototype was able to provide better cooling performance as compared to higher evaporator pressures. Lastly, as mentioned earlier, the cooling performance decreases, as evaporator pressure increases.

The better cooling performance provided by isopropyl alcohol as compared to water can be explained through vapor pressure of respective fluids. To elaborate further on vapor pressure, it can be defined as a measure of the intermolecular forces between within the compound (Voutsas, 2007). Hence, a compound with a weaker bond strength will tend to vaporise faster, which resulted in a higher vapor pressure, and vice versa. At any given temperature,

the fluid with higher vapor pressure is said to be more volatile, because the fluid will have higher rate of evaporation (Speight, 2020). The correlation between evaporation rate and vapor pressure was also studied by Mackay and Van Wesenbeeck (2014); Van Wesenbeeck, Driver and Ross (2008). Both of the studies concluded that the natural logarithm of evaporation rate versus the natural logarithm of vapor pressure shows a coefficient of determination (r^2) of 0.99, which shows that evaporation rate of a substance is strongly positive correlated to its vapor pressure.

From Figure 4.6 at any given temperature, the vapor pressure of isopropyl alcohol is higher than water. This shows that at the same ambient temperature and evaporator pressure, isopropyl alcohol will evaporate faster than water implying that isopropyl alcohol is more volatile as compared to water. Hence, when isopropyl alcohol is used as working fluid, the prototype is able to transfer more heat as compared to water, due to the higher evaporation rate of isopropyl alcohol.

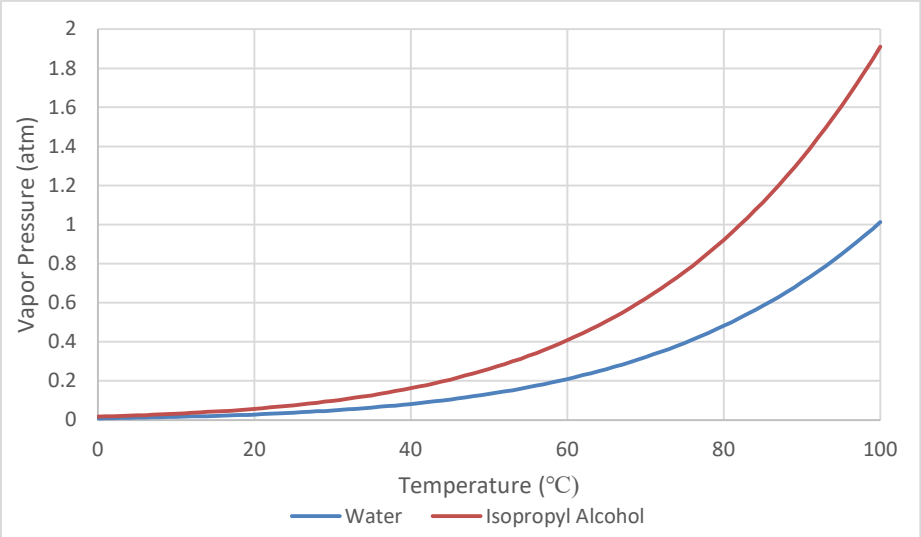

Figure 4.6: Graph of vapor pressure against temperature of water and isopropyl alcohol.

As mentioned earlier, the prototype was able to achieve better cooling performance at lower evaporator pressure as compared to higher evaporator pressure. This observation can be associated to the rate of evaporation of the working fluid. As the evaporator pressure decreases, the evaporation rate

increases. Özgür and Koçak (2015); Kitahara et al. (2014) performed studies on the effect of atmospheric pressure on the evaporation of water and concluded that evaporation rate will increase with the decreased in atmospheric pressure. Kazemi, Nobes and Elliott (2017) also performed an experimental study on the effect of pressure inside a chamber on evaporation rate and also concluded that as pressure inside the chamber decreased, the evaporation rate increased. The increase in evaporation rate can further be explained mathematically, through the diffusion coefficient derived from Boltzmann equation shown in Equation 4.5 (Sefiane et al., 2009).

$$D_{AB} = 0.00266 \frac{f_D T^{\frac{3}{2}}}{P M_{AB}^{\frac{1}{2}} \sigma_{AB}^{\frac{1}{2}} \Omega_D} \tag{4.5}$$

Where

$D_{AB} = diffusion\ coeffiecient\ of\ gas\ A\ into\ gas\ B$

$M_A = molecular\ weight\ of\ gas\ A$

$M_B = molecular\ weight\ of\ gas\ B$

$M_{AB} = 2\left(\frac{1}{M_A} + \frac{1}{M_B}\right)^{-1}$

$T = absolute\ temperature$

$P = Pressure$

$\sigma_{AB} = characteristic\ length\ associated\ with\ size\ of\ diffusing\ molecules$

$\Omega_D = diffusion\ collision\ integral$

$f_D = corrective\ term$

From Equation 4.5, it can be deduced that the diffusion coefficient is inversely proportional to pressure, while proportional to $T^{3/2}$. Assuming that at a short period of time, the temperature inside the evaporator does not fluctuate widely, hence as pressure inside the evaporator decreased, the diffusion coefficient of working fluid will increase, leading to an increased rate of evaporation. The amount of heat removed by evaporation can be determined using Equation 4.6.

$$Q = m\Delta H_{vap} \tag{4.6}$$

Where

$Q = amount\ of\ heat\ removed\ from\ liquid\ working\ fluid$

$m = mass\ of\ working\ fluid\ evaporated$

$\Delta H_{vap} = latent\ heat\ of\ vaporization$

Equation 4.6 shows that when the mass of working fluid evaporated increase, due to the increasing evaporation rate, the amount of heat removed will increase, leading to a better cooling performance in lower pressures.

As aforementioned in Chapter 3, the prototype reached its steady state after operating for 60 minutes. The steady state of the prototype was defined as the state where the evaporator pressure remains constant for 2 consecutive temperature measurement period. The constant evaporator temperature indicated that there is no net cooling in the evaporator, therefore, it can be said that the prototype has reached its maximum cooling performance. From Equation 2.36, it is shown that the cooling capacity of air conditioner is calculated using the psychrometric properties of air. Alternatively, cooling capacity of a system can be calculated using the thermodynamic properties of the refrigerant or working fluid as shown in Equation 3.7 and 4.6. From Equation 4.6, the cooling capacity is dependent on the latent heat of vaporization and mass of working fluid evaporated. Because the latent heat of vaporization of a fluid is constant, hence the cooling capacity is constrained by the mass of evaporated working fluid. At a specific evaporator pressure, the diffusion coefficient will stay constant as illustrated in Equation 4.5, which in turn constrained the amount of working fluid evaporated. Therefore, at steady state, the rate of evaporation of the working fluid will determine the cooling capacity of the prototype.

Lastly, the cooling performance may also be physically limited by the structure of the prototype. In an ideal situation, the evaporator and condenser are two locations in which heat transfer will occur in the prototype. Based on the current evaporator design, the GI pipe has thick walls as compared to the helical coil copper tubes. This may present as an issue as the thicker the wall, the higher thermal resistance of the structure, indicating that the heat transfer will be reduced. This can be displayed mathematically through Equation 4.7 (Cengel and Ghajar, 2020).

$$\dot{Q} = \frac{T_{evap} - T_{amb}}{R_{conv} + R_{cond}} \quad (4.7)$$

Where

$T_{evap} = temperature\ inside\ the\ evaporator$

$T_{amb} = ambient\ temperature$

$$R_{conv} = \frac{1}{h_1(2\pi r_1 L)} \quad (4.8)$$

$$R_{cond} = \frac{\ln\left(\frac{r_2}{r_1}\right)}{2\pi L k_1} \quad (4.9)$$

From Equation 4.7, assuming the driving force, which is the difference in T_{evap} and T_{amb} remains the same. While the convection resistance, R_{conv} of the heat transfer is constant. Hence, heat transfer will depend on the conduction resistance, R_{cond}. For the evaporator of the same length (L) and material (k), the resistance of conduction will depend on the $\ln(r_2/r_1)$, where r_2 and r_1 is the outer and inner radius of the evaporator respectively. It can be observed that when wall thickness increases the resistance due to conduction increases, leading to a decrease in heat transfer rate. Although the HPAC maybe rated for higher rate of heat transfer, the thermal resistance of the evaporator may physically limit the cooling performance of the prototype.

4.4 Summary

From the experiment, the concept of HPAC was successfully proven. This is because at low evaporator pressure, large ΔT over time was observed when isopropyl alcohol was used as working fluid, which indicated that the prototype had perform cooling. Isopropyl alcohol performed better in terms of cooling as compared to water. This is due to the higher vapor pressure of isopropyl alcohol as compared to water, which presented isopropyl alcohol as a more volatile working fluid. Although it can be seen that in Equation 4.6, latent heat of vaporization of the working fluid will impact the cooling capacity of the prototype. However, the enthalpy of vaporization for both working fluid only

differed by 800 J/mol $\left(\Delta H_{vap_{water}} = 40650 \frac{J}{mol}; \Delta H_{vap_{IPA}} = 39850 \frac{J}{mol}\right)$. Therefore, in this experiment, the evaporation rate played a more significant role in cooling performance in contrast to latent heat of vaporization. Because isopropyl alcohol is able to vaporise easier, hence it increased the cooling capacity of the prototype significantly. The pressure also affect the cooling performance of the prototype by controlling the diffusion coefficient of the working fluid, which in turn controlled the evaporation rate. The diffusion coefficient of the working fluid will increase with the decreased in pressure, hence at lower pressure, the working fluid is able to evaporate faster, leading to an increase in heat transfer rate. Overall, the prototype performed better when isopropyl alcohol is used as working fluid. The prototype achieved its maximum cooling performance at evaporator pressure of 26 kPa, when isopropyl alcohol is used as working fluid.

CHAPTER 5

CONCLUSION AND RECOMMENDATIONS

5.1 Conclusions

The completion of this final year project reveals that the concept of HPAC is possible. This indicates that both of the objectives were achieved. To reiterate, the objectives of this final year project are:

1. To model the use of heat pipe for air conditioning application.
2. To design and develop a proof of concept model of the heat pipe air conditioning system.

The first objective of the final year project is achieved by analysing the thermodynamic cycle of the HPAC shown in Chapter 3.2.1. The results from mathematical modelling can be concluded in Table 5.1. Assuming the ambient temperature is $30\ °C$.

Table 5.1: Results from mathematical modelling.

Parameter	Tap Water	Isopropyl Alcohol
Saturated Evaporator Pressure	$3.1698\ kPa$	$5.8000\ kPa$
Saturated Evaporator Temperature	$25\ °C$	$25\ °C$
Saturated Condenser Pressure	$5.6291\ kPa$	$10.4000\ kPa$
Saturated Condenser Temperature	$35\ °C$	$35\ °C$
Heat Transfer Rate, $\dot{Q}_H$	$0.235\ kJ/s$	$0.072\ kJ/s$

Based on the mathematical modelling, for heat transfer to occur, the evaporator and condenser pressure has to be reduced to the respective saturated pressure at the indicated temperature. For example, when water is used as working fluid, to maintain the evaporator and condenser temperature at $25\ °C$ and $35\ °C$ respectively, the evaporator pressure has to be reduced to 3.1698 kPa (absolute pressure) and 5.6291 kPa (absolute pressure) for condenser. The heat absorption rate calculated when water is used as working fluid is 0.235 kJ/s while, isopropyl alcohol is 0.072 kJ/s.

The second objective of the final year project is achieved through constructing the prototype. The prototype showed a significant increase in ΔT over time at low evaporator pressure (absolute pressure: 26 kPa to 60 kPa), when isopropyl alcohol is used as working fluid, showing that the prototype had perform cooling. Through the experiment, it was also found that the cooling performance increased, as the evaporator pressure decreased. This is due to the increase in diffusion coefficient, which increased the evaporation rate, resulting in an increase in rate of heat transfer. Furthermore, it was discovered that isopropyl alcohol performed better cooling as compared to water. This is due to the higher volatility of isopropyl alcohol as compared to water. At the same temperature, the vapor pressure of isopropyl alcohol is higher than water. Because vapor pressure has a strongly positive correlation to the evaporation rate of a fluid, hence, it can be concluded that at the same temperature, isopropyl alcohol will have a higher evaporation rate as compared to water. Therefore, isopropyl alcohol is able to provide more cooling performance as compared to water.

Lastly, the prototype had the best cooling performance when the evaporator pressure is at 26 kPa (absolute pressure) and when isopropyl alcohol is used. This is because the ΔT over time is recorded at $2.5\ °C$, which is the highest among all other conditions. To summarise, both the objectives of this final year project are fulfilled and the concept of HPAC is successfully proven.

5.2 Recommendations for future work

As mentioned in Chapter 1.5, there are many factors which will affect the heat transfer capability of the prototype. For future work, there are a few recommendations as listed below

1. The evaporator can be further improved in terms of its structure and material to increase the heat transfer rate. This can be achieved by increasing the diameter of the evaporator chamber to allow for a larger liquid-vapor interface and decreasing the thickness of the evaporator wall. Cooling fins can also be added to increase the surface area for heat transfer.

2. Fill ratio can be altered to examine the effect on the heat transfer rate.
3. Although, in this experiment, different evaporator pressure were tested. However, the lowest evaporator pressure achieved was 26 kPa, due to insufficient vacuum evacuation. Therefore, a better vacuum evacuation mechanism can be developed to achieve lower evaporator pressure. This can be done by using a vacuum pump used in the HVAC industry to pull a vacuum in the HVAC system.
4. During preliminary testing, it was also found that the prototype could not perform cooling. This may be due to the large influx of heat from the environment, which exceeded the cooling capacity of the prototype. Hence, foam insulation was used to isolate the evaporator from the environment. The recommendation is to thermally insulate the transfer lines and fittings to prevent excessive heat from entering the prototype, which may increase the cooling performance of the prototype.
5. Lastly, in this experiment, only two fluids were used as the working fluid, which are isopropyl alcohol and water. The effect of high vapor pressure fluids such as ammonia, ethane and methane on the heat transfer rate can be examined.

REFERENCES

Abdelaziz, G.B., Abdelbaky, M.A., Halim, M.A., Omara, M.E., Elkhaldy, I.A., Abdullah, A.S., Omara, Z.M., Essa, F.A., Ali, A., Sharshir, S.W., El-Said, E.M.S., Bedair, A.G. and Kabeel, A.E., 2021. Energy saving via heat pipe heat exchanger in air conditioning applications "experimental study and economic analysis." *Journal of Building Engineering*, [e-journal] 35. https://doi.org/10.1016/j.jobe.2020.102053.

Abdul Mujeebu, M., 2019. Introductory Chapter: Indoor Environmental Quality. In: *Indoor Environmental Quality*. IntechOpen.

Abdullahi, B., Al-dadah, R. and Mahmoud, S., 2019. Thermosyphon Heat Pipe Technology. In: *Recent Advances in Heat Pipes [Working Title]*. IntechOpen.p.13.

Akanmu, W.P., Nunayon, S.S. and Eboson, U.C., 2021. Indoor environmental quality (IEQ) assessment of Nigerian university libraries: A pilot study. *Energy and Built Environment*, [e-journal] 2(3), pp.302–314. https://doi.org/10.1016/J.ENBENV.2020.07.004.

Alhuyi Nazari, M., Ahmadi, M.H., Ghasempour, R., Shafii, M.B., Mahian, O., Kalogirou, S. and Wongwises, S., 2018. A review on pulsating heat pipes: From solar to cryogenic applications. *Applied Energy*, [e-journal] 222, pp.475–484. https://doi.org/10.1016/j.apenergy.2018.04.020.

Ambirajan, A., Adoni, A.A., Vaidya, J.S., Rajendran, A.A., Kumar, D. and Dutta, P., 2012. Loop heat pipes: A review of fundamentals, operation, and design. *Heat Transfer Engineering*, [e-journal] 33(4), pp.387–405. https://doi.org/10.1080/01457632.2012.614148.

Amir, A., Farid Mohamed, M., Khairul Azhar Mat Sulaiman, M. and Fatimah Mohammad Yusoff, W., 2019. Assessment of indoor thermal condition of a low-cost single story detached house: A case study in Malaysia. *Alam Cipta*, 12, pp.80–88.

Aono, Y., Watanabe, N., Ueno, A. and Nagano, H., 2021. Development of a loop heat pipe with kW-class heat transport capability. *Applied Thermal Engineering*, [e-journal] 183, p.116169. https://doi.org/10.1016/J.APPLTHERMALENG.2020.116169.

Arifin, N.A. and Denan, Z., 2015. An analysis of indoor air temperature and relative humidity in office room with various external shading devices in Malaysia. *Procedia - Social and Behavioral Sciences*, [e-journal] 179. https://doi.org/10.1016/j.sbspro.2015.02.432.

ASHRAE, 2010. *ASHRAE Standards 55: Thermal Environmental Conditions for Human Occupancy*.

Asumadu-Sakyi, A.B., Barnett, A.G., Thai, P.K., Jayaratne, E.R., Miller, W., Thompson, M.H., Rahman, M.M. and Morawska, L., 2021. Determination of the association between indoor and outdoor temperature in selected houses and its application: a pilot study. *Advances in Building Energy Research*, [e-journal] 15(5). https://doi.org/10.1080/17512549.2019.1606732.

Baharum, M.A., Surat, M., Tawil, N.M. and Che-Ani, A.I., 2014. Modern Housing Tranquillity in Malaysia from the Aspect of Thermal Comfort for Humid Hot Climate Zone. *E3S Web of Conferences*, 3.

Barba, M., Bruce, R., Bouchet, F., Bonelli, A. and Baudouy, B., 2021. Effects of filling ratio of a long cryogenic Pulsating Heat Pipe. *Applied Thermal Engineering*, [e-journal] 194(5). https://doi.org/10.1016/j.applthermaleng.2021.117072.

Barbosa, M. and Mantelli, H., 2021. *Thermosyphons and Heat Pipes: Theory and Applications*. Springer.

Barrak, A., 2021. Heat Pipes Heat Exchanger for HVAC Applications. In: *Heat Transfer - Design, Experimentation and Applications*. IntechOpen.

Bavishi, N. and Raiyani, H., 2017. Design and CFD analysis of liquid ring vacuum pump. *International Journal of Advance Engineering and Research*, 4(4), pp.457–464.

Bernagozzi, M., Georgoulas, A., Miché, N., Rouaud, C. and Marengo, M., 2021. Novel battery thermal management system for electric vehicles with a loop heat pipe and graphite sheet inserts. *Applied Thermal Engineering*, [e-journal] 194, p.117061. https://doi.org/10.1016/J.APPLTHERMALENG.2021.117061.

Bokoch, M.P. and Weston, S.D., 2020. *Inhaled Anesthetics: Delivery Systems*. Ninth Edit ed. *Miller's Anesthesia 9th ed*. Elsevier.

Borgnakke, C. and Sonntag, R.E., 2019. *Fundamentals of Thermodynamics*. 10th ed. Hoboken: John Wiley & Sons, Inc.

Cai, B., Deng, W., Wu, T., Wang, T., Ma, Z., Liu, W., Ma, L. and Liu, Z., 2021. Experimental study of a loop heat pipe with direct pouring porous wick for cooling electronics. *Processes*, [e-journal] 9(8), pp.1332–1347. https://doi.org/10.3390/pr9081332.

Capozzoli, A. and Primiceri, G., 2015. Cooling systems in data centers: State of art and emerging technologies. In: *Energy Procedia*. Elsevier Ltd.pp.484–493.

Cedeño Laurent, J.G., Williams, A., Oulhote, Y., Zanobetti, A., Allen, J.G. and Spengler, J.D., 2018. Reduced cognitive function during a heat wave among residents of non-air-conditioned buildings: An observational study of young adults in the summer of 2016. *PLOS Medicine*, [e-journal] 15(7). https://doi.org/10.1371/journal.pmed.1002605.

Cengel, Y. and Bole, M., 2015. *Thermodynamics An Engineering Approach*. Eight ed. New York: McGraw-Hill Education.

Cengel, Y. and Ghajar, A., 2020. *Heat and Mass Transfer: Fundamentals & Applications*. 6th ed. New York: McGraw-Hill Education.

Chua, K.J., Ng, K.C., Islam, M.R. and Shahzad, M.W., 2021. *Advances in Air Conditioning Technologies*. First ed. Singapore: Springer Nature Singapore Pte Ltd.

Demirel, Y., 2018. 5.2 Energy Conservation. In: *Comprehensive Energy Systems*. Elsevier.pp.45–90.

Department of Standards Malaysia, 2014. *Energy efficiency and use of renewable energy for non-residential buildings-Code of practice (Second revision)*.

Dincer, I. and Rosen, M.A., 2013. Exergy Analysis of Heat Pump Systems. In: *Exergy*, Second. Elsevier.pp.101–113.

Edreis, E. and Petrov, A., 2020. Types of heat exchangers in industry, their advantages and disadvantages, and the study of their parameters. In: *IOP Conference Series: Materials Science and Engineering*. IOP Publishing Ltd.

Eidan, A.A., Alshukri, M.J., Al-Fahham, M., Alsahlani, A. and Abdulridha, D.M., 2021. Optimizing the performance of the air conditioning system using an innovative heat pipe heat exchanger. *Case Studies in Thermal Engineering*, [e-journal] 26. https://doi.org/10.1016/j.csite.2021.101075.

Enke, C., Bertoldo Júnior, J. and Vlassov, V., 2021. Transient response of an axially-grooved aluminum-ammonia heat pipe with the presence of non-condensable gas. *Applied Thermal Engineering*, [e-journal] 183, p.116135. https://doi.org/10.1016/J.APPLTHERMALENG.2020.116135.

Esfandiari, M., Mohamed Zaid, S., Ismail, M.A., Reza Hafezi, M., Asadi, I., Mohammadi, S., Vaisi, S. and Aflaki, A., 2021. Occupants' satisfaction toward indoor environment quality of platinum green-certified office buildings in tropical climate. *Energies*, [e-journal] 14(8). https://doi.org/10.3390/en14082264.

Firouzfar, E., Soltanieh, M., Noie, S.H. and Saidi, M.H., 2012. Investigation of heat pipe heat exchanger effectiveness and energy saving in air conditioning systems using silver nanofluid. *International Journal of Environmental Science and Technology*, [e-journal] 9(4), pp.587–594. https://doi.org/10.1007/s13762-012-0051-9.

Gabsi, I., Maalej, S. and Zaghdoudi, M.C., 2018. Thermal performance modeling of loop heat pipes with flat evaporator for electronics cooling. *Microelectronics Reliability*, [e-journal] 84, pp.37–47. https://doi.org/10.1016/J.MICROREL.2018.02.023.

Ganesh, G.A., Sinha, S.L., Verma, T.N. and Dewangan, S.K., 2021. Investigation of indoor environment quality and factors affecting human comfort: A critical review. *Building and Environment*, [e-journal] 204, p.108146. https://doi.org/https://doi.org/10.1016/j.buildenv.2021.108146.

Geng, Y., Ji, W., Lin, B. and Zhu, Y., 2017. The impact of thermal environment on occupant IEQ perception and productivity. *Building and Environment*, [e-journal] 121. https://doi.org/10.1016/j.buildenv.2017.05.022.

Guo, C., 2019. The Recent Research of Loop Heat Pipe. In: *Recent Advances in Heat Pipes [Working Title]*. IntechOpen. https://doi.org/10.5772/intechopen.85408.

Hamdan, M. and Elnajjar, E., 2009. Thermodynamic analytical model of a loop heat pipe. *Heat and Mass Transfer*, [e-journal] 46(2), pp.167–173. https://doi.org/10.1007/s00231-009-0555-0.

Harrison, G. and Marlton, G., 2020. Pressure on the boiling point. *Weather*, [e-journal] 75(4). https://doi.org/10.1002/wea.3693.

He, J., Miao, J., Bai, L., Lin, G., Zhang, H. and Wen, D., 2017. Effect of non-condensable gas on the startup of a loop heat pipe. *Applied Thermal Engineering*, [e-journal] 111, pp.1507–1516. https://doi.org/10.1016/j.applthermaleng.2016.07.154.

Holloway, P.H. and Pritchard, D.G., 2017. Effects of ambient temperature and water vapor on chamber pressure and oxygen level during low atmospheric pressure stunning of poultry. *Poultry Science*, [e-journal] 96(8), pp.2528–2539. https://doi.org/10.3382/ps/pex066.

Htoo, K.Z., Huynh, P.H., Kariya, K. and Miyara, A., 2021. Experimental study on thermal performance of a loop heat pipe with different working wick materials. *Energies*, [e-journal] 14(9), pp.2453–2475. https://doi.org/10.3390/en14092453.

Jamaludin, N., Mohammed, N.I., Khamidi, M.F. and Wahab, S.N.A., 2015. Thermal comfort of residential building in Malaysia at different micro-climates. *Procedia - Social and Behavioral Sciences*, [e-journal] 170, pp.613–623. https://doi.org/10.1016/j.sbspro.2015.01.063.

Jin, T.X., 2007. Experimental investigation of the temperature variation in the vacuum chamber during vacuum cooling. *Journal of Food Engineering*, [e-journal] 78(1), pp.333–339. https://doi.org/10.1016/j.jfoodeng.2005.09.034.

Jose, J. and Baby, R., 2018. Recent advances in loop heat pipes: A review. In: *IOP Conference Series: Materials Science and Engineering*. pp.12060–12067.

Jouhara, H., 2018. Heat Pipes. *Comprehensive Energy Systems*, [e-journal] 4, pp.70–97. https://doi.org/10.1016/B978-0-12-809597-3.00403-X.

Jouhara, H. and Meskimmon, R., 2018. An investigation into the use of water as a working fluid in wraparound loop heat pipe heat exchanger for applications in energy efficient HVAC systems. *Energy*, [e-journal] 156, pp.597–605. https://doi.org/10.1016/j.energy.2018.05.134.

Kazemi, M.A., Nobes, D.S. and Elliott, J.A.W., 2017. Experimental and numerical study of the evaporation of water at low pressures. *Langmuir*, [e-journal] 33(18), pp.4578–4591. https://doi.org/10.1021/acs.langmuir.7b00616.

Kirkham, M.B., 2014. Chapter 3 - Structure and Properties of Water. In: M.B. Kirkham, ed. *Principles of Soil and Plant Water Relations (Second Edition)*. Boston: Academic Press.pp.27–40.

Kishi, R. and Araki, A., 2020. Indoor Environmental Quality and Health Risk toward Healthier Environment for All. In: R. Kishi, D. Norback and A. Araki, eds. *Indoor Environmental Quality and Health Risk toward Healthier Environment for All*. Singapore: Springer Nature Singapore Pte Ltd.pp.3–18.

Kitahara, M., Ozawa, H., Kodama, A., Izukura, H., Inoue, S. and Uchida, K., 2014. Effect of atmospheric pressure on hearing in normal subjects. *Journal of Arid Land Studies*, [e-journal] 22(1), pp.303–306. https://doi.org/10.3109/00016489409127310.

Koh, K., Al-Kayiem, H.H. and Kurnia, J.C., 2018. Thermal Comfort Assessment of an Office Building in Tropical Climate Condition. *MATEC Web of Conferences*, 225.

Ku, J., 2016. Loop Heat Pipe Startup Behaviors. In: *46th International Conference on Environmental Systems*.

Legg, R., 2017. *Air conditioning system design*. First ed. Kidlington: Elsevier Ltd.

Liberty, J.T., Ugwuishiwu, B.O., Pukuma, S. a. and Odo, C.E., 2013. Principles and application of evaporative cooling systems for fruits and vegetables preservation. *International Journal of Current Engineering and Technology*, 3(3), pp.1000–1006.

Mackay, D. and Van Wesenbeeck, I., 2014. Correlation of chemical evaporation rate with vapor pressure. *Environmental Science and Technology*, [e-journal] 48(17), pp.10259–10263. https://doi.org/10.1021/es5029074.

Manimaran, R., Palaniradja, K., Alagumurthi, N. and Hussain, J., 2019. Factors affecting the thermal performance of heat pipe-A review. *Global Journal of Engineering Science and Research Management*, 6(3), pp.12–17.

Maydanik, Y.F., 2005. Loop heat pipes. *Applied Thermal Engineering*, [e-journal] 25, pp.635–657. https://doi.org/10.1016/j.applthermaleng.2004.07.010.

Mendes, A. and Teixeira, J.P., 2014. Sick Building Syndrome. In: *Encyclopedia of Toxicology*. Elsevier.

Meseguer; Jose, Grande; Isabel Perez and Andres; Angel Sanz, 2012. *spacecraft thermal control*. First ed. Cambridge: Elsevier Science.

MyGovernment, 2016. *Malaysia Information: Climate*. [online] Available at: <https://www.malaysia.gov.my/portal/content/144> [Accessed 29 September 2021].

Nakkaew, S., Chitipalungsri, T., Ahn, H.S., Jerng, D.W., Asirvatham, L.G., Dalkiliç, A.S., Mahian, O. and Wongwises, S., 2019. Application of the heat pipe to enhance the performance of the vapor compression refrigeration system. *Case Studies in Thermal Engineering*, [e-journal] 15. https://doi.org/10.1016/j.csite.2019.100531.

NCT, 2021. *Heat Pipe for Thermal Management*. [online] Available at: <https://www.1-act.com/innovations/heat-pipes/> [Accessed 28 August 2021].

Nguyen, J.L., Schwartz, J. and Dockery, D.W., 2014. The relationship between indoor and outdoor temperature, apparent temperature, relative humidity, and absolute humidity. *Indoor Air*, [e-journal] 24(1). https://doi.org/10.1111/ina.12052.

Ormandy, D. and Ezratty, V., 2016. Thermal discomfort and health: protecting the susceptible from excess cold and excess heat in housing. *Advances in Building Energy Research*, [e-journal] 10(1). https://doi.org/10.1080/17512549.2015.1014845.

Özgür, E. and Koçak, K., 2015. The effects of the atmospheric pressure on evaporation. *Acta Geobalcanica*, [e-journal] 1(1), pp.17–24. https://doi.org/10.18509/agb.2015.02.

Qu, J., Wu, H., Cheng, P., Wang, Q. and Sun, Q., 2017. Recent advances in MEMS-based micro heat pipes. *International Journal of Heat and Mass Transfer*, [e-journal] 110, pp.294–313. https://doi.org/10.1016/j.ijheatmasstransfer.2017.03.034.

Rahman, L., Chowdhury, M., Aeslan Islam, N., Muhammad Mufti, S. and Ali, M., 2016. Effect of filling ratio and orientation of closed loop pulsating heat pipe using ethanol. In: *AIP Conference Procedings*. pp.050011-1-050011–7.

Rani, M.F.H., Razlan, Z.M., Shahriman, A.B., Zunaidi, I., Wan, W.K., Hashim, M.S.M., Ibrahim, I., Kamarrudin, N.S., Ayob, R. and Noramzil, N.N.A., 2018. Cooling capacity of 1 HP room air conditioner - Comparison between indoor room testing condition of ISO 5151 standard requirement and average Malaysian preferable condition. In: *IOP Conference Series: Materials Science and Engineering*. Institute of Physics Publishing.pp.12070–12075.

Reay, D.A., Kew, P.A. and McGlen, R.J., 2014a. Heat transfer and fluid flow theory. In: *Heat Pipes*. Elsevier.pp.15–64.

Reay, D.A., Kew, P.A. and McGlen, R.J., 2014b. Special types of heat pipe. In: *Heat Pipes*. Elsevier.pp.135–173.

Reji, A.K., Kumaresan, G., Sarathi, A., Arasappa, G.P.S., Kumar, R.S. and Matthew, M.S., 2021. Analysis of thermosiphon working with eco-friendly refrigerant under various fill ratios. *Materials Today: Proceedings*, [e-journal] 45(2), pp.2618–2621. https://doi.org/10.1016/J.MATPR.2020.10.1013.

Scalabrin, G. and Stringari, P., 2009. A fundamental equation of state for 2-propanol (C3 H8 O) in the extended equation of state format. *Journal of Physical and Chemical Reference Data*, [e-journal] 38(2), pp.127–170. https://doi.org/10.1063/1.3112608.

Schweiker, M., Huebner, G.M., Kingma, B.R.M., Kramer, R. and Pallubinsky, H., 2018. Drivers of diversity in human thermal perception – A review for holistic comfort models. *Temperature*, [e-journal] 5(4). https://doi.org/10.1080/23328940.2018.1534490.

Sefiane, K., Wilson, S.K., David, S., Dunn, G.J. and Duffy, B.R., 2009. On the effect of the atmosphere on the evaporation of sessile droplets of water. *Physics of Fluids*, [e-journal] 21(6). https://doi.org/10.1063/1.3131062.

Setyawan, I., Putra, N., Hakim, I.I. and Irwansyah, R., 2019. Development of hybrid loop heat pipe using pump assistance for cooling application on high heat flux device. *Journal of Mechanical Science and Technology*, [e-journal] 33(8), pp.3685–3694. https://doi.org/10.1007/s12206-019-0710-6.

Sforza, P.M., 2017. Quasi-One-Dimensional Flow Equations. In: *Theory of Aerospace Propulsion*, 2nd ed. Elsevier.pp.53–84.

Shafieian, A. and Khiadani, M., 2020. Integration of heat pipe solar water heating systems with different residential households: An energy, environmental, and economic evaluation. *Case Studies in Thermal Engineering*, [e-journal] 21, p.100662. https://doi.org/10.1016/J.CSITE.2020.100662.

Shahsavar Goldanlou, A., Kalbasi, R. and Afrand, M., 2020. Energy usage reduction in an air handling unit by incorporating two heat recovery units. *Journal of Building Engineering*, [e-journal] 32, p.101545. https://doi.org/10.1016/J.JOBE.2020.101545.

Sharma, C. and Sharma, S., 2019. A Review of Heat Pipes: its types and applications. *International Journal of Engineering Research & Technology*, 8(03), pp.103–106.

Shinko Electric Industries, 2021. *Micro Loop Heat Pipe*. [online] Available at: <https://www.shinko.co.jp/english/product/thermal/m3hp.php> [Accessed 13 August 2021].

Shioga, T. and Mizuno, Y., 2015. Micro loop heat pipe for mobile electronics applications. In: *31st Thermal Measurement, Modeling & Management Symposium (SEMI-THERM)*. IEEE.

Smitka, M., Kolková, Z., Nemec, P. and Malcho, M., 2014. Impact of the amount of working fluid in loop heat pipe to remove waste heat from electronic component. In: *EPJ Web of Conferences 67*. pp.02109-1-02109–4.

Speight, J.G., 2017. Chapter 5 - Properties of Organic Compounds. In: J.G. Speight, ed. *Environmental Organic Chemistry for Engineers*. Butterworth-Heinemann.pp.203–261.

Speight, J.G., 2020. *The properties of water*. *Natural Water Remediation*,

Su, Q., Chang, S., Song, M., Zhao, Y. and Dang, C., 2019. An experimental study on the heat transfer performance of a loop heat pipe system with ethanol-water mixture as working fluid for aircraft anti-icing. *International Journal of Heat and Mass Transfer*, [e-journal] 139, pp.280–292. https://doi.org/10.1016/J.IJHEATMASSTRANSFER.2019.05.015.

Subiantoro, A., Ooi, K.T. and Junaidi, A.Z., 2013. Performance and suitability comparisons of some R22 possible substitute refrigerants. In: *Institution of Mechanical Engineers - 8th International Conference on Compressors and Their Systems*. Woodhead Publishing.pp.67–76.

Sundén, B. and Fu, J., 2017. *Heat transfer in aerospace applications*. First ed. Oxford: Elsevier.

Suruhanjaya Tenaga, 2018. *GUIDE ON MINIMUM ENERGY PERFORMANCE STANDARD REQUIREMENTS FOR AIR CONDITIONER WITH COOLING CAPACITY ≤ 7.1kW*.

Tharayil, T., Asirvatham, L.G., Ravindran, V. and Wongwises, S., 2016. Effect of filling ratio on the performance of a novel miniature loop heat pipe having different diameter transport lines. *Applied Thermal Engineering*, [e-journal] 106, pp.588–600. https://doi.org/10.1016/j.applthermaleng.2016.05.125.

Toyinbo, O., 2019. Indoor Environmental Quality. *Indoor Environmental Quality [Working Title]*, pp.107–122.

Voutsas, E., 2007. *Estimation of the Volatilization of Organic*. *Thermodynamics solubility and environmental issues*. Elsevier B.V.

Wai Tuck, N., Ahmad Zaki, S., Hagishima, A., Bahadur Rijal, H., Azuan Zakaria, M. and Yakub, F., 2019. Investigation of indoor thermal environments in a two-story corner terrace house in Malaysia. *KnE Social Sciences*.

Wallin, P., 2012. Heat Pipe, selection of working fluid. *Heat and Mass Transfer*, 160.

Wan, H., Cao, T., Hwang, Y. and Oh, S., 2020. A review of recent advancements of variable refrigerant flow air-conditioning systems. *Applied Thermal Engineering*, [e-journal] 169, p.114893. https://doi.org/10.1016/J.APPLTHERMALENG.2019.114893.

Wang, C., Zhang, F., Wang, J., Doyle, J.K., Hancock, P.A., Mak, C.M. and Liu, S., 2021. How indoor environmental quality affects occupants' cognitive functions: A systematic review. *Building and Environment*, [e-journal] 193, p.107647. https://doi.org/https://doi.org/10.1016/j.buildenv.2021.107647.

Wang, H., Lin, G., Shen, X., Bai, L. and Wen, D., 2019. Effect of evaporator tilt on a loop heat pipe with non-condensable gas. *International Journal of Heat and Mass Transfer*, [e-journal] 128, pp.1072–1080. https://doi.org/10.1016/J.IJHEATMASSTRANSFER.2018.09.033.

Van Wesenbeeck, I., Driver, J. and Ross, J., 2008. Relationship between the evaporation rate and vapor pressure of moderately and highly volatile chemicals. *Bulletin of Environmental Contamination and Toxicology*, [e-journal] 80(4), pp.315–318. https://doi.org/10.1007/s00128-008-9380-2.

Xie, M., Xue, Z., Qu, W. and Li, W., 2015. Experimental investigation of heat transfer performance of rotating heat pipe. *Procedia Engineering*, [e-journal] 99, pp.746–751. https://doi.org/10.1016/j.proeng.2014.12.597.

Xu, Z., Zhang, Y., Li, B., Wang, C.C. and Ma, Q., 2018. Heat performances of a thermosyphon as affected by evaporator wettability and filling ratio. *Applied Thermal Engineering*, [e-journal] 129, pp.665–673. https://doi.org/10.1016/J.APPLTHERMALENG.2017.10.073.

Yang, D. and Mak, C.M., 2020. Relationships between indoor environmental quality and environmental factors in university classrooms. *Building and Environment*, [e-journal] 186, p.107331. https://doi.org/https://doi.org/10.1016/j.buildenv.2020.107331.

Yusoff, W.F.M. and Ja'afar, N.H., 2019. Preliminary evaluation of indoor thermal comfort in Malaysia heritage mosque. *MATEC Web of Conferences*, 277.

Zaki, S.A., Hanip, N.F.M., Hagishima, A., Yakub, F. and Ali, M.S.M., 2018. Survey of resident behaviour related to air conditioner operation in low-cost apartments of Kuala Lumpur. *Chemical Engineering Transactions*, [e-journal] 63, pp.259–264. https://doi.org/10.3303/CET1863044.

Zhang, H., Jiang, C., Zhang, Z., Liu, Z., Luo, X. and Liu, W., 2020a. A study on thermal performance of a pump-assisted loop heat pipe with ammonia as working fluid. *Applied Thermal Engineering*, [e-journal] 175, p.115342. https://doi.org/10.1016/J.APPLTHERMALENG.2020.115342.

Zhang, Y., Xia, Z., Song, B., Xu, M., Tian, Y. and Chen, Y., 2020b. Experimental analysis on the loop heat pipes with different microchannel evaporators. *Applied Thermal Engineering*, [e-journal] 178, p.115547. https://doi.org/10.1016/J.APPLTHERMALENG.2020.115547.

Zhang, Z., Zhao, R., Liu, Z. and Liu, W., 2021. Application of biporous wick in flat-plate loop heat pipe with long heat transfer distance. *Applied Thermal Engineering*, [e-journal] 184, p.116283. https://doi.org/10.1016/j.applthermaleng.2020.116283.

Zhou, F., Wei, C. and Ma, G., 2017. Development and analysis of a pump-driven loop heat pipe unit for cooling a small data center. *Applied Thermal Engineering*, [e-journal] 124, pp.1169–1175. https://doi.org/10.1016/J.APPLTHERMALENG.2017.06.108.

Zohuri, B., 2016. *Heat Pipe Design and Technology Modern Applications for Practical Thermal Management*. Second ed. Switzerland: Springer International Publishing.

Zohuri, Bahman., 2020. *Functionality, advancements and industrial applications of heat pipes*. First ed. Oxford: Academic Press.

APPENDICES

Appendix A: Additional Discussion

During preliminary testing, it was found that the helical coil copper tube could not perform well as an evaporator. When the helical coil copper tube is used as an evaporator, the working fluid can be seen sloshing inside the polyurethane pipe from the copper tube as shown in Figure A.1. Two links to videos showed the sloshing of the working fluid can be found below. (https://drive.google.com/file/d/1HRQFZVuFZEyeya-nd5RhxXEnT1y2W-dm/view?usp=sharing https://drive.google.com/file/d/1HHOVyPfiPCg0M57xbdl5JMd2ngs-jYJG/view?usp=sharing).

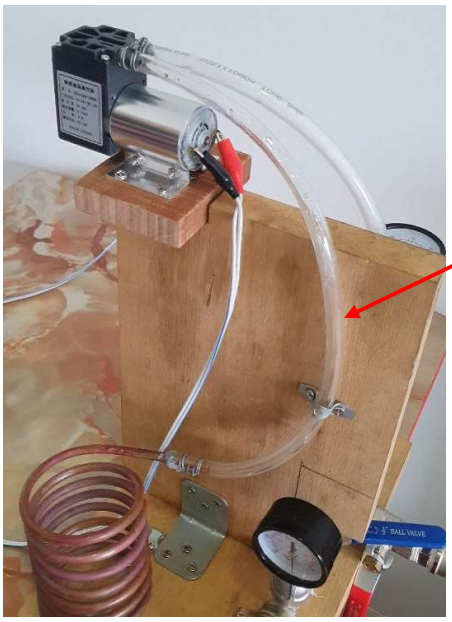

Figure A. 1: Location of working fluid sloshing

Because of the sloshing action, it is assumed that the working fluid cannot evaporate properly. Therefore, in order to solve the evaporation issue, a chamber which has a larger surface area is used instead. The chamber used has a 2-inch inner diameter, in comparison to the 0.21-inch inner diameter of the copper pipe. The larger surface area exposes more of the liquid working fluid

to the air, increasing the liquid-air interface, which facilitates the evaporation of working fluid.

Because there are no complete data of vapor pressure for isopropyl alcohol, the graph in Figure 4.6 was plotted using the Clausius-Clapeyron equation shown in Equation A.1.

$$\ln\left(\frac{P_1}{P_2}\right) = \frac{\Delta H_{vap}}{R}\left(\frac{1}{T_2} - \frac{1}{T_1}\right) \qquad (A.1)$$

Where

$P_1 = vapor\ pressure\ at\ state\ 1$

$P_2 = vapor\ pressure\ at\ state\ 2$

$T_1 = Temperature\ at\ state\ 1$

$T_2 = Temperature\ at\ state\ 2$

$\Delta H_{vap} = latent\ heat\ of\ vaporization$

$R = Gas\ Constant$

Arranging Equation A.1 will generate Equation A.2.

$$P_1 = e^{\frac{\Delta H_{vap}}{R}\left(\frac{1}{T_2} - \frac{1}{T_1}\right) - lnP_2} \qquad (A.2)$$

The graph of vapor pressure against temperature is plotted using Equation 5.2. The graph shown in Figure 4.6 was plotted with the resolution of $1°C$ for isopropyl alcohol and water.

Appendix B: Tables

Table B.1: Temperature data for evaporator pressure at 26 kPa (Working fluid: Isopropyl Alcohol)

Time (min)	$T_{evap}(°C)$	T_{cond} $(°C)$	T_{amb} $(°C)$	ΔT $(°C)$
0	29.5	30.0	30.3	0.8
20	28.8	30.3	29.7	0.9
40	27.3	29.9	29.6	2.3
60	27.0	30.1	29.5	2.5

Table B.2: Temperature data for evaporator pressure at 30 kPa (Working fluid: Isopropyl Alcohol)

Time (min)	T_{evap} $(°C)$	T_{cond} $(°C)$	$T_{amb}(°C)$	ΔT $(°C)$
0	28.6	29.1	29.1	0.5
20	27.9	29.6	29.1	1.2
40	27.6	29.3	29.1	1.5
60	27.4	29.3	29.2	1.8

Table B.3: Temperature data for evaporator pressure at 40 kPa (Working fluid: Isopropyl Alcohol)

Time (min)	T_{evap} $(°C)$	T_{cond} $(°C)$	$T_{amb}(°C)$	ΔT $(°C)$
0	28.2	28.5	28.6	0.4
20	27.8	29.4	29.0	1.2
40	27.5	29.9	29.2	1.7
60	27.5	30.1	29.3	1.8

Table B.4: Temperature data for evaporator pressure at 60 kPa (Working fluid: Isopropyl Alcohol)

Time (min)	T_{evap} $(°C)$	T_{cond} $(°C)$	$T_{amb}(°C)$	ΔT $(°C)$
0	29.9	30.4	30.4	0.5
20	29.5	31.2	30.9	1.4
40	29.2	31.3	30.6	1.4
60	29.1	31.1	30.5	1.4

Table B.5: Temperature data for evaporator pressure at 80 kPa (Working fluid: Isopropyl Alcohol)

Time (min)	T_{evap} $(°C)$	T_{cond} $(°C)$	$T_{amb}(°C)$	ΔT $(°C)$
0	29.8	30.1	30.2	0.4
20	29.8	30.4	30.3	0.5
40	29.8	30.3	30.2	0.4
60	29.8	29.9	29.8	0

Table B.6: Temperature data for evaporator pressure at 100 kPa (Working fluid: Isopropyl Alcohol)

Time (min)	T_{evap} (°C)	T_{cond} (°C)	T_{amb}(°C)	ΔT (°C)
0	29.1	29.1	29.2	0.1
20	29.1	29.5	29.5	0.4
40	29.1	29.5	29.5	0.4
60	29.1	29.5	29.5	0.4

Table B.7: Temperature data for evaporator pressure at 26 kPa (Working fluid: Water)

Time (min)	T_{evap} (°C)	T_{cond} (°C)	T_{amb}(°C)	ΔT (°C)
0	28.6	30.1	30.3	1.7
20	28.6	30.2	30.3	1.7
40	28.9	30.9	30.6	1.7
60	29	31.1	30.8	1.8

Table B.8: Temperature data for evaporator pressure at 30 kPa (Working fluid: Water)

Time (min)	T_{evap} (°C)	T_{cond} (°C)	T_{amb}(°C)	ΔT (°C)
0	29.9	30.3	30.7	0.8
20	29.9	30.8	30.8	0.9
40	29.9	30.6	30.7	0.8
60	30	30.6	30.6	0.6

Table B.9: Temperature data for evaporator pressure at 40 kPa (Working fluid: Water)

Time (min)	T_{evap} (°C)	T_{cond} (°C)	T_{amb}(°C)	ΔT (°C)
0	30	30.1	30.1	0.1
20	29.8	30.1	30.1	0.3
40	29.8	30.1	30.1	0.3
60	29.8	30.1	30	0.2

Table B.10: Temperature data for evaporator pressure at 60 kPa (Working fluid: Water)

Time (min)	T_{evap} (°C)	T_{cond} (°C)	T_{amb}(°C)	ΔT (°C)
0	29.8	30.1	30.3	0.5
20	29.8	30.4	30.3	0.5
40	29.8	30.6	30.6	0.8
60	29.8	30.5	30.4	0.6

Table B.11: Temperature data for evaporator pressure at 80 kPa (Working fluid: Water)

Time (min)	T_{evap} (°C)	T_{cond} (°C)	T_{amb}(°C)	ΔT (°C)
0	29.7	29.6	29.6	-0.1
20	29.8	29.9	29.9	0.1
40	29.9	29.9	29.9	0
60	29.8	30	29.9	0.1

Table B.12: Temperature data for evaporator pressure at 100 kPa (Working fluid: Water)

Time (min)	T_{evap} (°C)	T_{cond} (°C)	T_{amb}(°C)	ΔT (°C)
0	29.6	29.6	29.6	0
20	29.6	30.6	30.3	0.7
40	29.8	31	30.3	0.5
60	30.1	31.1	30.6	0.5

Table B.13:Saturated Water (temperature) table (Cengel and Bole, 2015)

TABLE A–4

Saturated water—Temperature table

		Specific volume, m³/kg		Internal energy, kJ/kg			Enthalpy, kJ/kg			Entropy, kJ/kg·K		
Temp., T °C	Sat. press., P_{sat} kPa	Sat. liquid, v_f	Sat. vapor, v_g	Sat. liquid, u_f	Evap., u_{fg}	Sat. vapor, u_g	Sat. liquid, h_f	Evap., h_{fg}	Sat. vapor, h_g	Sat. liquid, s_f	Evap., s_{fg}	Sat. vapor, s_g
0.01	0.6117	0.001000	206.00	0.000	2374.9	2374.9	0.001	2500.9	2500.9	0.0000	9.1556	9.1556
5	0.8725	0.001000	147.03	21.019	2360.8	2381.8	21.020	2489.1	2510.1	0.0763	8.9487	9.0249
10	1.2281	0.001000	106.32	42.020	2346.6	2388.7	42.022	2477.2	2519.2	0.1511	8.7488	8.8999
15	1.7057	0.001001	77.885	62.980	2332.5	2395.5	62.982	2465.4	2528.3	0.2245	8.5559	8.7803
20	2.3392	0.001002	57.762	83.913	2318.4	2402.3	83.915	2453.5	2537.4	0.2965	8.3696	8.6661
25	3.1698	0.001003	43.340	104.83	2304.3	2409.1	104.83	2441.7	2546.5	0.3672	8.1895	8.5567
30	4.2469	0.001004	32.879	125.73	2290.2	2415.9	125.74	2429.8	2555.6	0.4368	8.0152	8.4520
35	5.6291	0.001006	25.205	146.63	2276.0	2422.7	146.64	2417.9	2564.6	0.5051	7.8466	8.3517
40	7.3851	0.001008	19.515	167.53	2261.9	2429.4	167.53	2406.0	2573.5	0.5724	7.6832	8.2556
45	9.5953	0.001010	15.251	188.43	2247.7	2436.1	188.44	2394.0	2582.4	0.6386	7.5247	8.1633
50	12.352	0.001012	12.026	209.33	2233.4	2442.7	209.34	2382.0	2591.3	0.7038	7.3710	8.0748
55	15.763	0.001015	9.5639	230.24	2219.1	2449.3	230.26	2369.8	2600.1	0.7680	7.2218	7.9898
60	19.947	0.001017	7.6670	251.16	2204.7	2455.9	251.18	2357.7	2608.8	0.8313	7.0769	7.9082
65	25.043	0.001020	6.1935	272.09	2190.3	2462.4	272.12	2345.4	2617.5	0.8937	6.9360	7.8296
70	31.202	0.001023	5.0396	293.04	2175.8	2468.9	293.07	2333.0	2626.1	0.9551	6.7989	7.7540
75	38.597	0.001026	4.1291	313.99	2161.3	2475.3	314.03	2320.6	2634.6	1.0158	6.6655	7.6812
80	47.416	0.001029	3.4053	334.97	2146.6	2481.6	335.02	2308.0	2643.0	1.0756	6.5355	7.6111
85	57.868	0.001032	2.8261	355.96	2131.9	2487.8	356.02	2295.3	2651.4	1.1346	6.4089	7.5435
90	70.183	0.001036	2.3593	376.97	2117.0	2494.0	377.04	2282.5	2659.6	1.1929	6.2853	7.4782
95	84.609	0.001040	1.9808	398.00	2102.0	2500.1	398.09	2269.6	2667.6	1.2504	6.1647	7.4151
100	101.42	0.001043	1.6720	419.06	2087.0	2506.0	419.17	2256.4	2675.6	1.3072	6.0470	7.3542
105	120.90	0.001047	1.4186	440.15	2071.8	2511.9	440.28	2243.1	2683.4	1.3634	5.9319	7.2952
110	143.38	0.001052	1.2094	461.27	2056.4	2517.7	461.42	2229.7	2691.1	1.4188	5.8193	7.2382
115	169.18	0.001056	1.0360	482.42	2040.9	2523.3	482.59	2216.0	2698.6	1.4737	5.7092	7.1829
120	198.67	0.001060	0.89133	503.60	2025.3	2528.9	503.81	2202.1	2706.0	1.5279	5.6013	7.1292
125	232.23	0.001065	0.77012	524.83	2009.5	2534.3	525.07	2188.1	2713.1	1.5816	5.4956	7.0771
130	270.28	0.001070	0.66808	546.10	1993.4	2539.5	546.38	2173.7	2720.1	1.6346	5.3919	7.0265
135	313.22	0.001075	0.58179	567.41	1977.3	2544.7	567.75	2159.1	2726.9	1.6872	5.2901	6.9773
140	361.53	0.001080	0.50850	588.77	1960.9	2549.6	589.16	2144.3	2733.5	1.7392	5.1901	6.9294
145	415.68	0.001085	0.44600	610.19	1944.2	2554.4	610.64	2129.2	2739.8	1.7908	5.0919	6.8827
150	476.16	0.001091	0.39248	631.66	1927.4	2559.1	632.18	2113.8	2745.9	1.8418	4.9953	6.8371
155	543.49	0.001096	0.34648	653.19	1910.3	2563.5	653.79	2098.0	2751.8	1.8924	4.9002	6.7927
160	618.23	0.001102	0.30680	674.79	1893.0	2567.8	675.47	2082.0	2757.5	1.9426	4.8066	6.7492
165	700.93	0.001108	0.27244	696.46	1875.4	2571.9	697.24	2065.6	2762.8	1.9923	4.7143	6.7067
170	792.18	0.001114	0.24260	718.20	1857.5	2575.7	719.08	2048.8	2767.9	2.0417	4.6233	6.6650
175	892.60	0.001121	0.21659	740.02	1839.4	2579.4	741.02	2031.7	2772.7	2.0906	4.5335	6.6242
180	1002.8	0.001127	0.19384	761.92	1820.9	2582.8	763.05	2014.2	2777.2	2.1392	4.4448	6.5841
185	1123.5	0.001134	0.17390	783.91	1802.1	2586.0	785.19	1996.2	2781.4	2.1875	4.3572	6.5447
190	1255.2	0.001141	0.15636	806.00	1783.0	2589.0	807.43	1977.9	2785.3	2.2355	4.2705	6.5059
195	1398.8	0.001149	0.14089	828.18	1763.6	2591.7	829.78	1959.0	2788.8	2.2831	4.1847	6.4678
200	1554.9	0.001157	0.12721	850.46	1743.7	2594.2	852.26	1939.8	2792.0	2.3305	4.0997	6.4302

Table B.14:Saturated Isopropyl Alcohol (temperature) table (Scalabrin and Stringari, 2009)

T (K)	p^{sat} (MPa)	ρ (kg m^{-3})	H (kJ kg^{-1})	S (kJ kg^{-1} K^{-1})	C_v (kJ kg^{-1} K^{-1})	C_p (kJ kg^{-1} K^{-1})	w (m s^{-1})
280.0	0.0017	796.80	216.00	1.0579	2.0120	2.3779	1221.2
		4.4471×10^{-2}	991.99	3.8299	1.2800	1.4193	206.91
282.0	0.0020	795.17	220.78	1.0749	2.0322	2.4029	1211.9
		5.1082×10^{-2}	994.80	3.8196	1.2874	1.4269	207.55
284.0	0.0023	793.53	225.62	1.0919	2.0530	2.4283	1202.7
		5.8894×10^{-2}	997.63	3.8103	1.2948	1.4344	208.19
286.0	0.0026	791.87	230.50	1.1091	2.0741	2.4541	1193.5
		6.6707×10^{-2}	1000.5	3.8013	1.3022	1.4420	208.82
288.0	0.0030	790.20	235.43	1.1263	2.0956	2.4802	1184.3
		7.6322×10^{-2}	1003.3	3.7925	1.3097	1.4496	209.45
290.0	0.0035	788.52	240.42	1.1435	2.1175	2.5067	1175.1
		8.6538×10^{-2}	1006.2	3.7840	1.3171	1.4573	210.06
292.0	0.0039	786.82	245.46	1.1608	2.1397	2.5334	1166.0
		9.7956×10^{-2}	1009.0	3.7759	1.3245	1.4650	210.67
294.0	0.0045	785.11	250.56	1.1782	2.1621	2.5603	1156.8
		0.110 58	1011.9	3.7679	1.3320	1.4727	211.27
296.0	0.0051	783.38	255.70	1.1957	2.1848	2.5875	1147.7
		0.124 40	1014.8	3.7602	1.3395	1.4804	211.87
298.0	0.0058	781.64	260.91	1.2132	2.2077	2.6149	1138.7
		0.140 02	1017.7	3.7528	1.3469	1.4882	212.45
300.0	0.0065	779.89	266.16	1.2308	2.2308	2.6425	1129.6
		0.157 45	1020.6	3.7456	1.3544	1.4960	213.03
302.0	0.0074	778.12	271.48	1.2484	2.2540	2.6702	1120.6
		0.176 68	1023.5	3.7385	1.3618	1.5038	213.59
304.0	0.0083	776.34	276.85	1.2661	2.2773	2.6980	1111.7
		0.197 72	1026.4	3.7319	1.3693	1.5117	214.15
306.0	0.0093	774.55	282.27	1.2839	2.3007	2.7259	1102.7
		0.221 15	1029.4	3.7254	1.3767	1.5196	214.70
308.0	0.0104	772.74	287.75	1.3018	2.3240	2.7539	1093.9
		0.246 99	1032.3	3.7191	1.3842	1.5276	215.23
310.0	0.0117	770.92	293.29	1.3197	2.3474	2.7819	1085.1
		0.274 64	1035.2	3.7130	1.3916	1.5356	215.76
312.0	0.0131	769.08	298.88	1.3377	2.3707	2.8098	1076.3
		0.305 29	1038.2	3.7071	1.3990	1.5436	216.27
314.0	0.0146	767.23	304.53	1.3557	2.3939	2.8378	1067.6
		0.338 94	1041.1	3.7014	1.4064	1.5516	216.77
316.0	0.0163	765.36	310.24	1.3738	2.4169	2.8657	1059.0
		0.375 60	1044.0	3.6959	1.4137	1.5597	217.26
318.0	0.0181	763.48	316.00	1.3920	2.4398	2.8935	1050.4
		0.415 86	1047.0	3.6906	1.4208	1.5676	217.74
320.0	0.0201	761.58	321.81	1.4102	2.4625	2.9212	1041.8
		0.459 73	1049.9	3.6855	1.4274	1.5751	218.21
322.0	0.0223	759.67	327.68	1.4285	2.4849	2.9488	1033.4
		0.507 21	1052.8	3.6805	1.4327	1.5814	218.68
324.0	0.0247	757.74	333.61	1.4468	2.5071	2.9762	1024.9
		0.558 29	1055.8	3.6757	1.4381	1.5825	219.18
326.0	0.0273	755.80	339.59	1.4652	2.5290	3.0034	1016.6
		0.614 18	1058.7	3.6709	1.4431	1.5644	219.83
328.0	0.0301	753.84	345.63	1.4837	2.5505	3.0305	1008.3
		0.674 88	1061.5	3.6661	1.4506	1.5684	220.34
330.0	0.0332	751.86	351.72	1.5021	2.5717	3.0573	1000.0
		0.740 38	1064.3	3.6616	1.4609	1.6158	220.48
332.0	0.0365	749.87	357.86	1.5207	2.5925	3.0838	991.81
		0.810 70	1067.2	3.6574	1.4711	1.6276	220.86
334.0	0.0401	747.86	364.06	1.5393	2.6129	3.1102	983.65
		0.887 02	1070.1	3.6533	1.4784	1.6366	221.25
336.0	0.0440	745.83	370.31	1.5579	2.6329	3.1362	975.55
		0.969 35	1073.0	3.6493	1.4860	1.6462	221.62
338.0	0.0482	743.78	376.61	1.5766	2.6524	3.1620	967.50
		1.0577	1075.9	3.6454	1.4941	1.6562	221.98
340.0	0.0528	741.72	382.96	1.5953	2.6715	3.1875	959.49
		1.1526	1078.7	3.6416	1.5024	1.6668	222.32
342.0	0.0577	739.64	389.37	1.6141	2.6901	3.2126	951.53
		1.2548	1081.5	3.6380	1.5112	1.6779	222.65
344.0	0.0630	737.53	395.82	1.6329	2.7082	3.2375	943.60
		1.3642	1084.4	3.6345	1.5204	1.6895	222.96
346.0	0.0686	735.41	402.32	1.6517	2.7257	3.2620	935.72
		1.4814	1087.2	3.6310	1.5300	1.7017	223.26
348.0	0.0747	733.27	408.88	1.6706	2.7428	3.2862	927.87
		1.6064	1090.0	3.6277	1.5400	1.7146	223.53
350.0	0.0812	731.10	415.48	1.6895	2.7593	3.3100	920.05
		1.7410	1092.7	3.6245	1.5506	1.7281	223.79
352.0	0.0882	728.92	422.12	1.7084	2.7752	3.3335	912.26
		1.8840	1095.5	3.6214	1.5616	1.7423	224.03
354.0	0.0957	726.71	428.82	1.7273	2.7907	3.3566	904.50
		2.0367	1098.3	3.6184	1.5732	1.7573	224.25
356.0	0.1037	724.48	435.56	1.7463	2.8055	3.3794	896.76
		2.1995	1101.0	3.6155	1.5853	1.7729	224.45

Appendix C: CAD Drawings

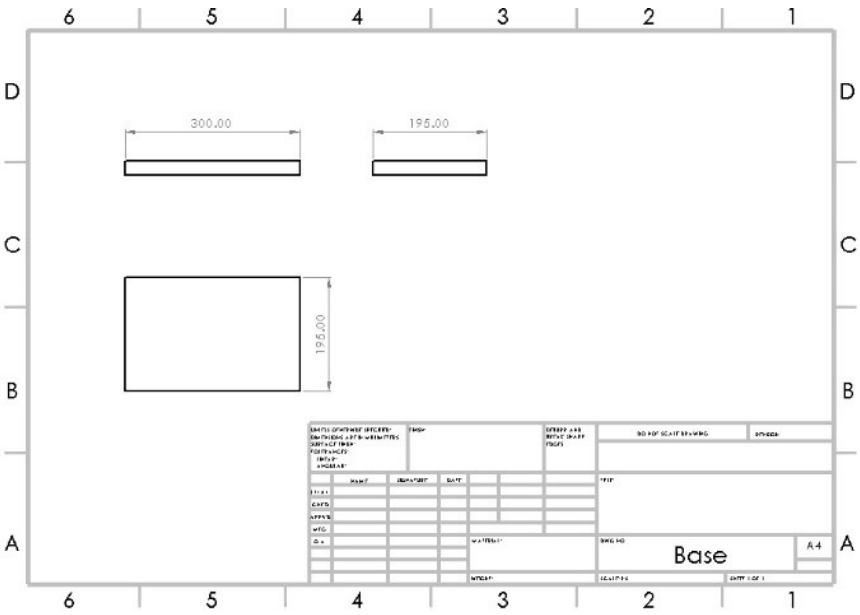

Figure C. 1: Dimension of the base

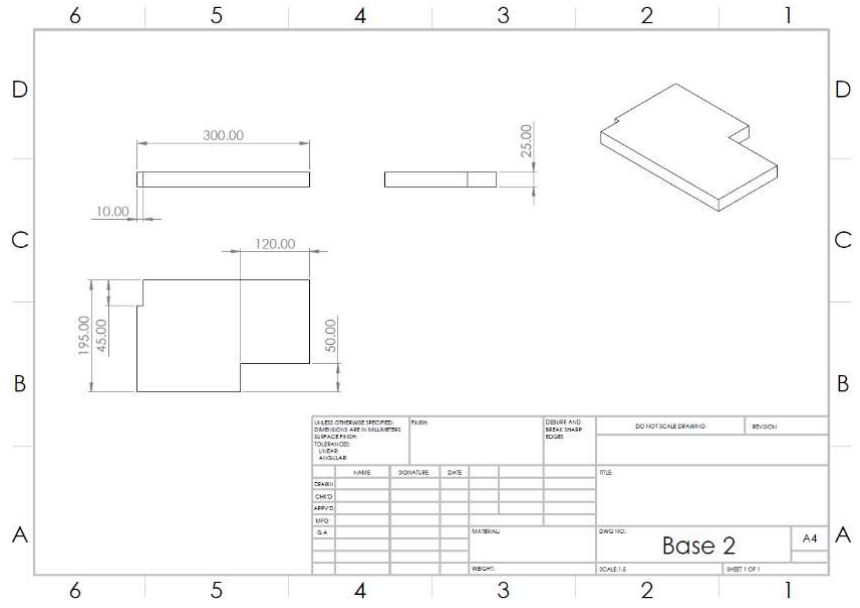

Figure C. 2: Dimension of the vertical platform

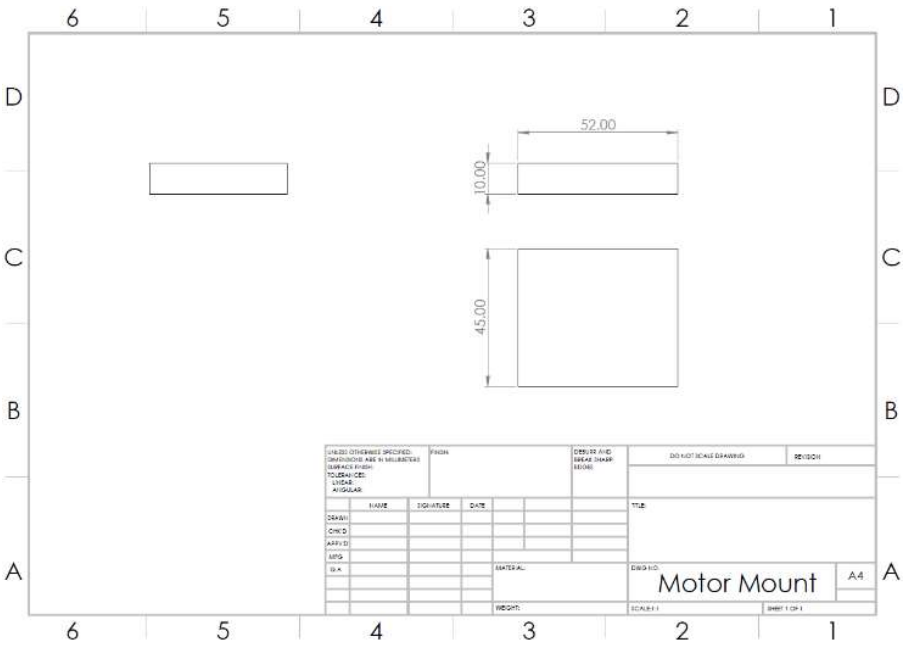

Figure C. 3: Dimension of the motor mount

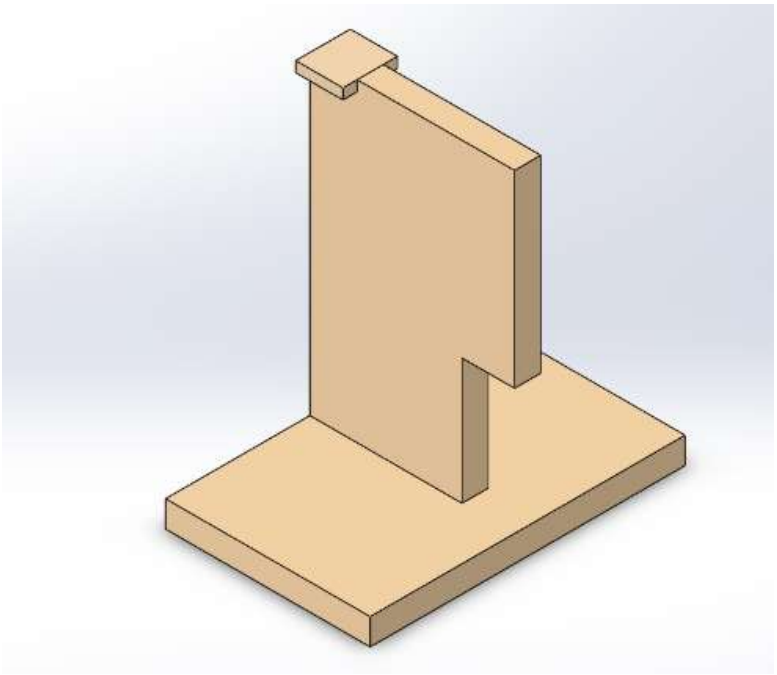

Figure C. 4: Isometric view of complete platform

Appendix D: Workplan

The work plan for the final year project part 1 and part is summarised in the Gantt Chart show in Table D.1 and D.2.

Table D.1: Gantt Chart for FYP 1

No.	Project Activities	W1	W2	W3	W4	W5	W6	W7
M1	Project Planning with supervisor							
M2	Literature Review							
M3	Report Writing							
M4	Report Submission and Presentation							

Table D.1: Gantt Chart for FYP 1 (continued)

No.	Project Activities	W8	W9	W10	W11	W12	W13	W14
M1	Project Planning with supervisor							
M2	Literature Review							
M3	Report Writing							
M4	Report Submission and Presentation							

Table D.2: Gantt Chart for FYP 2

No.	Project Activities	W1	W2	W3	W4	W5	W6	W7
M1	Prototyping (Fabrication, Assembly)							
M2	Prototyping (Testing, Commissioning)							
M3	Report Writing							
M4	Report Submission & Presentation							

Table D.2: Gantt Chart for FYP 2 (continued)

No	Project Activities	W8	W9	W 10	W 11	W 12	W 13	W 14
M1	Prototyping (Fabrication, Assembly)							
M2	Prototyping (Testing, Commissioning)							
M3	Report Writing							
M4	Report Submission & Presentation							